CERN-ACC-NOTE-2019-0042

March 2019

Report and Analysis from LHC MD 3311: Amplitude detuning at end-of-squeeze

J. Dilly, M. Albert, T. Argyropoulos, F. Carlier, M. Hofer, L. Malina, E. H. Maclean, M. Solfaroli Camillocci, R. Tomás

Keywords: LHC, amplitude detuning, K-Modulation

Summary

Amplitude detuning at *end-of-squeeze* is measured during this MD, with both flat-orbit and crossing-angles in IP5. These measurements are conducted to be able to identify the source of the detuning found during commissioning in 2018. Further, results from simulations are compared to the measured detuning. A test for the K-modulation measurement is also run during the MD.

Contents

1 History and Motivation

The linear action-dependent tune shift in a storage ring is called first-order amplitude detuning and has significant impact on the tune footprint of accelerator beams, affecting dynamic aperture and beam stability [1]. It consists of two *direct* terms $\partial Q_x/\partial(2J_x)$ and $\partial Q_y/\partial(2J_y)$, and the *cross* term $\partial Q_x/\partial(2J_y) = \partial Q_y/\partial(2J_x)$ [2]. In first order, these terms are generated by normal octupole fields [3, 4].

As octupole fields are also generated through feed-down [5], applying crossing angles in the machine at low β^*-optics will have significant repercussions on amplitude detuning.

First assessments of amplitude detuning at injection energy in the LHC were established as early as 2011, utilizing free kicks. The detuning was mitigated parasitically by second-order chromaticity corrections using the main dipoles' spool pieces [6, 7].

In 2012 the measurement method was improved by making use of the AC-Dipole (ACD), and then applied at injection- and top-energy [8, 9, 10, 11].

After the first long shutdown, commissioning in 2015 included a repetition of the chromaticity corrections at injection energy from 2011, thus verifying the reduction of amplitude detuning [12].

During 2016's commissioning, amplitude detuning was studied for the first time at $\beta^* = 40\,\text{cm}$ and results were used to correct for normal octupolar field errors in IR1 and IR5. To separate the effects between the IRs, simulations based on magnetic error measurements of the magnets [13, 14] and feed-down to tune, measured via crossing-angle scans, were taken into account. In addition, comparison with the simulations showed the measured octupole errors in IR5 to be smaller than expected, demanding further investigation [15]. Later that year, the first detuning measurements with a crossing angle (185 µrad in IP5) were performed, but showed no significant difference to flat-orbit [16, 17]. Additional measurements of detuning were done, applying dedicated asymmetric orbit bumps to pin-point the location of the sources in IR5 [16]. Furthermore, the influence of coupling on amplitude detuning was also investigated that year and suggested to be responsible for discrepancies from second-order detuning measurements to simulations seen in 2012 [18].

For commissioning in 2017, amplitude detuning was again successfully corrected at flat-orbit following the octupole correction scheme established in 2016 [19], even though β^* was squeezed to a smaller value of 30 cm. In contrast to earlier commissioning, the detuning correction was now an integral part of the commissioning scheme, and linear corrections were re-evaluated after non-linear corrections [20, 21]. It was discovered during commissioning, that detuning increased when the full crossing scheme was applied. As octupole errors in IP5 were already excluded to produce feed-down to detuning due to the measurements from 2016, feed-down from IP1 errors were investigated during a Machine Development (MD) session later in 2017 at crossing angles of $\pm 150\,\mu\text{rad}$ and a β^* of 40 cm. Yet, the origin of the seen detuning could not be determined, as the measured detuning terms were small [22]. At the end of 2017 another MD was dedicated to measuring amplitude detuning during different stages at top-energy, namely before squeeze and at end-of-squeeze ($\beta^* = 30\,\text{cm}$) without crossing angles, and end-of-squeeze with the full operational crossing scheme of 2017 applied [23]. The end-of-squeeze measurements showed significant increase in detuning upon applying the crossing angles, even with the commissioning corrections applied.

2018 commissioning followed the new nonlinear-linear correction scheme introduced in 2017 [20, 21]. At the end of commissioning, detuning measurements with full crossing scheme were repeated and residual detuning, similar to what was seen in 2017, was verified [24, 25]. Results of that measurement are shown for comparison in Section 2.4. Table 1 shows that the measured detuning could be corrected by a split of 250 A in Beam 1 and 57 A in Beam 2 in powering of the focussing (MOF) and defocusing (MOD) Landau octupole families. Strong detuning of this strength has the potential to affect instabilities at various points during the squeeze. Since the source of the detuning is not understood, it is not possible to predict how the tune footprint will vary.

MD3311 was launched to help understand observed instabilities in the machine and to investigate new sources for amplitude detuning, explaining the disagreement between measurements and magnetic model seen in 2016. A full summary of all amplitude detuning measurements can be found in Table 2.

Further, the K-modulation software [26] was tested during the MD, as some measurements during commissioning (e.g. [27]) led to results with poor reproducibility. In particular, problems were encountered when orbit feedback was involved. Also, a dodecapolar resonance driving term (RDT) was probed to test the ability to measure RDTs of that order.

Table 1: Amplitude detuning during commissioning 2018 and the MO powering necessary for correction. The powering is given in absolute values, as the MO families are powered with opposite signs. The current default MO powering is $I_{MOF/MOD} = \pm\, 546\,\mathrm{A}$.

		LHCB 1			LHCB 2		
	MO-Type	Value	$\lvert I_{MO}\rvert$	$\Delta\lvert I_{MO}\rvert$	Value	$\lvert I_{MO}\rvert$	$\Delta\lvert I_{MO}\rvert$
	–	$[10^3\,\mathrm{m}^{-1}]$	[A]	[A]	$[10^3\,\mathrm{m}^{-1}]$	[A]	[A]
$\partial Q_x/\partial(2J_x)$	MOF	$+34 \pm 1$	431	-115	-5 ± 1	557	+11
$\partial Q_y/\partial(2J_y)$	MOD	-38 ± 1	681	+135	$+13 \pm 3$	500	-46
$\lvert I_{MOD} - I_{MOF}\rvert$		250 A			57 A		

Table 2: Summary of all amplitude detuning measurements from 2011-2018. Measurements for Beam 1 are shown in blue (top), for Beam 2 in red (bottom). Where AC-Dipole kicks were used, the results have been corrected for the effect of forced oscillations. Since 2017 comissioning b_4 corrections, using the multipolar correctors in the triplet [28], were in place.

[10^3 m^{-1}]	Case	$\partial Q_x/\partial(2J_x)$	$\partial Q_y/\partial(2J_x)$	$\partial Q_x/\partial(2J_y)$	$\partial Q_y/\partial(2J_y)$	Ref.
2011 flat-orbit, before Q'' corr.	Inj.	– -12.2 ± 0.2	– 8.4 ± 0.5	– 9.4 ± 1.3	– -2.5 ± 1.5	[6, 7]
2011 flat-orbit, after Q'' corr.	Inj.	– -2.9 ± 0.6	– 2.7 ± 1.7	– 0.6 ± 0.5	– 2.3 ± 0.8	[6, 7]
2012, MO on flat-orbit	Inj.	– -29 ± 7	– 19 ± 3	– 24 ± 4	– -32.8 ± 0.4	[8]
2012, MO off flat-orbit, Q''+Q''' corr.	Inj.	– 0.8 ± 1	– -1.4 ± 0.4	– -2 ± 0.7	– 2.8 ± 1	[8]
2012 flat-orbit	4 TeV β^*= 11 m	-0.1 ± 0.2 1 ± 1	0.5 ± 0.7 3 ± 1	– –	– –	[11]
2012 flat-orbit	4 TeV β^*= 0.6 m	– 9 ± 1	– -17 ± 4	– –	– –	[11]
2016 commissioning flat-orbit	6.5 TeV β^*= 0.4 m	43 ± 1 38 ± 1	– –	0.1 ± 1 0.3 ± 1	-50 ± 1 -44 ± 1	[16, 20]
2016 MD1391 flat-orbit	6.5 TeV β^*= 0.4 m	– –	– –	15 ± 5 10 ± 1	-42 ± 2 -43 ± 1	[16, 20]
2016 MD1391 IP5 +185 µrad	6.5 TeV β^*= 0.4 m	– 41 ± 1	– –	15 ± 5 7 ± 1	-50 ± 3 -44 ± 1	[16, 20]
2017 commissioning flat-orbit (b_4 corrected ↓)	6.5 TeV β^*= 0.3 m	-3 ± 1 -2 ± 1	5 ± 3 -3 ± 2	– –	– 2 ± 1	[29, 20]
2017 commissioning full crossing	6.5 TeV β^*= 0.4 m	– -3 ± 1	– 23 ± 4	– –	– –	[29]
2017 MD2158 IP1 -150 µrad	6.5 TeV β^*= 0.4 m	– 0.7 ± 0.7	– -11 ± 1	– –	– –	[29]
2017 MD2158 IP1 +150 µrad	6.5 TeV β^*= 0.4 m	– -3 ± 1	– -3 ± 1	– –	– –	[29]
2017 MD2723 flat-orbit	6.5 TeV β^*= 1 m	11 ± 3 2.5 ± 0.7	3 ± 2 -2 ± 2	2.5 ± 1.5 -1.9 ± 0.6	-3.8 ± 1.6 -1.7 ± 1.0	[23]
2017 MD2723 flat-orbit	6.5 TeV β^*= 0.3 m	– -1.1 ± 0.6	– -1 ± 2	– -2 ± 2	9 ± 2 -0.9 ± 1.2	[23]
2017 MD2723 full crossing	6.5 TeV β^*= 0.3 m	61 ± 15 0.4 ± 0.9	13 ± 8 -9 ± 3	– -25 ± 3	– 14 ± 2	[23]
2018 commissioning full cross. +160 µrad (Table 3)	6.5 TeV β^*= 0.3 m	34 ± 1 -3 ± 1	8 ± 2 -10 ± 3	18 ± 1 -14 ± 2	-38 ± 1 13 ± 3	[24, 25] Figs. 4 and 5
2018 MD3311 flat-orbit	6.5 TeV β^*= 0.3 m	0.8 ± 0.5 -7.5 ± 0.5	10 ± 1 8 ± 2	8 ± 28 -2 ± 1	-3 ± 1 6 ± 1	*new* Figs. 4 and 5
2018 MD3311 IP5 +160 µrad (Table 4)	6.5 TeV β^*= 0.3 m	56 ± 6 1.5 ± 0.5	-9 ± 15 4 ± 1	108 ± 24 -4 ± 3	3 ± 2 12 ± 1	*new* Figs. 4 and 5

Table 3: Settings for amplitude detuning measurements during comissioning on the 28.04.2018.

Fill #:	6619
Beam Process:	MD → SQUEEZE-6.5TeV-ATS-1m-30cm-2018_V1_MD0@638_[END]
Date:	28 . 04 . 2018
Start Time:	16 : 00
End Time:	18 : 00
Optics:	R2017aT_A30C30A10mL300_CTPPS2
Tunes:	$Q_x = 0.31$, $Q_y = 0.32$
Crossing:	[160 / 200 / 160 / -250] µrad in [IP1 / IP2 / IP5 / IP8], *Plane:* [V / V / H / H]
Separation:	[-0.55 / 1.4 / 0.55 / -1] mm in [IP1 / IP2 / IP5 / IP8], *Plane:* [H / H / V / V]

2 Measurement Summary

Table 4 summarizes the key parameters and the machine configuration of the MD.

Table 4: Key MD parameters.

Objective:	Analysis of the influence of IP5 crossing scheme on the amplitude detuning.
MD #:	3311
Operators:	Markus Albert, Theodoros Argyropoulos
Fill #:	6811
Beam Process:	MD → SQUEEZE-6.5TeV-ATS-1m-30cm-2018_V1_MD1@638_[END]
Date:	16 . 06 . 2018
Start Time:	15 : 45
End Time:	23 : 45
Optics:	R2017aT_A30C30A10mL300_CTPPS2
Tunes:	$Q_x = 0.31$, $Q_y = 0.32$ *(unless otherwise specified)*
Crossing:	[0 / 0 / 160 / 0] µrad in [IP1 / IP2 / IP5 / IP8], *Plane:* [V / V / H / H]
Separation:	[0 / 0 / 0.55 / 0] mm in [IP1 / IP2 / IP5 / IP8], *Plane:* [H / H / V / V]
Offset:	[0 / 0 / -1.8 / 0] mm in [IP1 / IP2 / IP5 / IP8], *Plane:* [V / V / H / H]

2.1 Procedure

Tables 5 and 6 detail the time line of the MD. As usual, coupling measurements via ACD and corrections were done after every change of machine state to exclude coupling as a source of amplitude detuning. The final coupling correction - after restoring crossing-angles and beam separation in IP5 - did not succeed. The reason for this failure is still unknown, as it has never happened before nor has it been seen again during later measurements. Coupling must have been relatively well corrected as no detrimental effects could be observed during the continuation of the MD.

Measurements were performed using again the ACD. At first, the standard collision tunes were utilized, with natural fractional tunes of $Q_x = 0.31$ and $Q_y = 0.32$. Yet, during flat-orbit horizontal kicks, a resonance line close to the natural tune became visible in the spectrum. It was later confirmed to be a decapolar resonance, induced by the vertical driven tune $Q_y^{ACD} = 0.33$. In Fig. 1 the resonance line (0,4) can be seen at $4Q_y^{ACD} = 1.32 \approx Q_y + 1$. Consequently, the natural tunes for Beam 1 were moved to $Q_x = 0.305$ and $Q_y = 0.315$, to avoid disruption of the natural tune measurements. The same tunes were again applied for Beam 1 during horizontal kicks with crossing angles later on, when the resonance line was seen again.

K-modulation and RDT measurements were also performed.

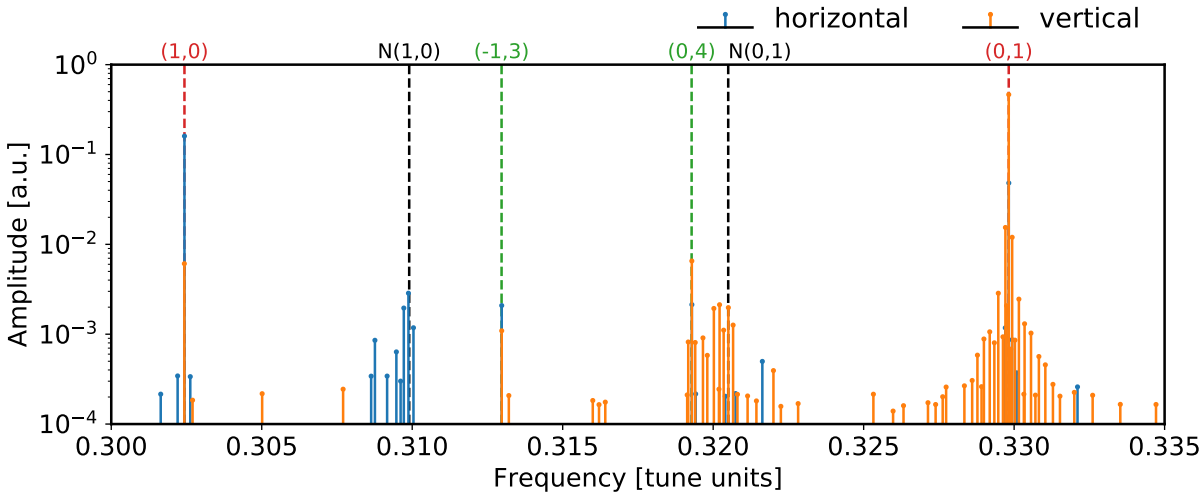

Figure 1: Beam 1 measured frequency spectrum of the horizontal and vertical plane with measured tunes and resonances. Driven tunes and resonance lines are marked as "(n_x, n_y)" referring to frequencies $f = (n_x Q_x^{ACD} + n_y Q_y^{ACD})$ mod 1 and $1 - f$ if $f > 0.5$. Natural tunes follow the same nomenclature preceded by the letter "N". $Q_y^{ACD} \approx 0.33$, i.e. (0,1), causes the decapolar resonance (0,4), which interferes with the measurement of the vertical natural tune N(0,1) close by: $4Q_y^{ACD}$ mod $1 \approx 0.32 \approx Q_y$. The resonance at (-1,3) did not disturb the measurement, as it was far away from the tunes.

Table 5: MD Time-line (Part 1). Key measurements are shown in **bold**.

15:45→17:30	Setting up beam to end-of-squeeze, nominal crossing-angles
17:30→17:48	Coupling Measurements:
	Beam 1: $+2.8 \cdot 10^{-3} - 1.4i \cdot 10^{-3}$
	Beam 2: $-0.7i \cdot 10^{-3}$
	⇒ correcting Beam 1:
	Beam 1: $-0.2i \cdot 10^{-3}$
17:48→18:49	**K-Mod with crossing-angles:**
	IP1, 5A, 2 Cycles, orbit feedback off
	IP1, 5A, 2 Cycles, orbit feedback and radial loop on
18:49	**Removed crossing-angles and separation bumps.**
	→ One orbit corrector failed.
	⇒ Small orbit error.
18:54→19:00	Coupling Measurements:
	Beam 1: $+3.0 \cdot 10^{-3} - 2.0i \cdot 10^{-3}$
	Beam 2: $-2.8i \cdot 10^{-3}$
	⇒ correcting Beam 1 and Beam 2:
	Beam 1: $-0.3 \cdot 10^{-3} - 0.3i \cdot 10^{-3}$
	Beam 2: $+0.6 \cdot 10^{-3} + 0.2i \cdot 10^{-3}$
19:00→19:20	**K-Mod at flat-orbit:**
	IP1, 5A, 2 Cycles
19:20→20:30	**Vertical kicks for flat-orbit amp. det.** (10% horizontal)
	→ Beam 2: Problems with Multiturn-GUI. Many restarts.
	→ Not properly logged in elogbook, but good in kickgroups.
20:30→21:30	**Horizontal kicks for flat-orbit amp. det.** (10% vertical)
	→ Beam 2: Problems with Multiturn-GUI. Like above.
20:57	→ Beam 1: Decapolar resonance showing up at natural tune line.
	⇒ changed tune for Beam 1 to $Q_x = 0.305, Q_y = 0.315$
21:30→21:35	Changing working point to $Q_x = 0.305, Q_y = 0.325$
	⇒ probing 5^{th} order resonance line $Q_x - 4Q_y = -1$

Table 6: MD Time-line (Part 2). Key measurements are shown in **bold**.

21:35→21:55	**Diagonal kicks for RDT measurements at flat-orbit.**
21:55→22:10	Restoring crossing angles and separation bumps.
	IP5-XING-H-MURAD $= 160$
	IP5-OFFSET-V-MM $= -1.8$
	IP5-SEP-V-MM $= 0.55$
22:10→23:00	Coupling Measurements:
	Beam 1: $-0.4 \cdot 10^{-3} - 1.4i \cdot 10^{-3}$
	Beam 2: $+0.5 \cdot 10^{-3} - 1.4i \cdot 10^{-3}$
	$\Rightarrow$ correcting Beam 1 and Beam 2:
	$\rightarrow$ **FAILED** for unknown reasons. Example values:
	Beam 1: $-2.7 \cdot 10^{-3} + 1.9i \cdot 10^{-3}$
	Beam 1: $+5.0 \cdot 10^{-3} - 3.4i \cdot 10^{-3}$
	Beam 2: $+0.4 \cdot 10^{-3} + 3.5i \cdot 10^{-3}$
	Beam 2: $+0.9 \cdot 10^{-3} - 5.9i \cdot 10^{-3}$
	$\Rightarrow$ correcting Beam 1 and Beam 2 again:
	$\rightarrow$ **FAILED** for unknown reasons. At least consistent signs:
	Beam 1: $-2.6 \cdot 10^{-3} + 1.1i \cdot 10^{-3}$
	Beam 2: $-1.0 \cdot 10^{-3} + 1.2i \cdot 10^{-3}$
23:00→23:30	**Vertical kicks for amp. det. with crossing-angles and bumps.** (10% horizontal)
	$\rightarrow$ Beam 2: Problems with Multiturn-GUI. Like above.
23:30→00:20	**Horizontal kicks for amp. det. with crossing-angles and bumps.** (10% vertical)
	$\rightarrow$ Beam 2: Problems with Multiturn-GUI. Like above.
23:45	$\rightarrow$ Beam 1: Decapolar resonance showing up. Like above.
	$\Rightarrow$ changed tune for Beam 1 to $Q_x = 0.305, Q_y = 0.315$

2.2 RDT Measurement Results

During this MD a dodecapolar RDT was probed by moving the working point close to a fifth-order resonance line, as shown in Fig. 2. The resonance is $Q_x - 4Q_y = -1$ and the results of the measurement are investigated in [30].

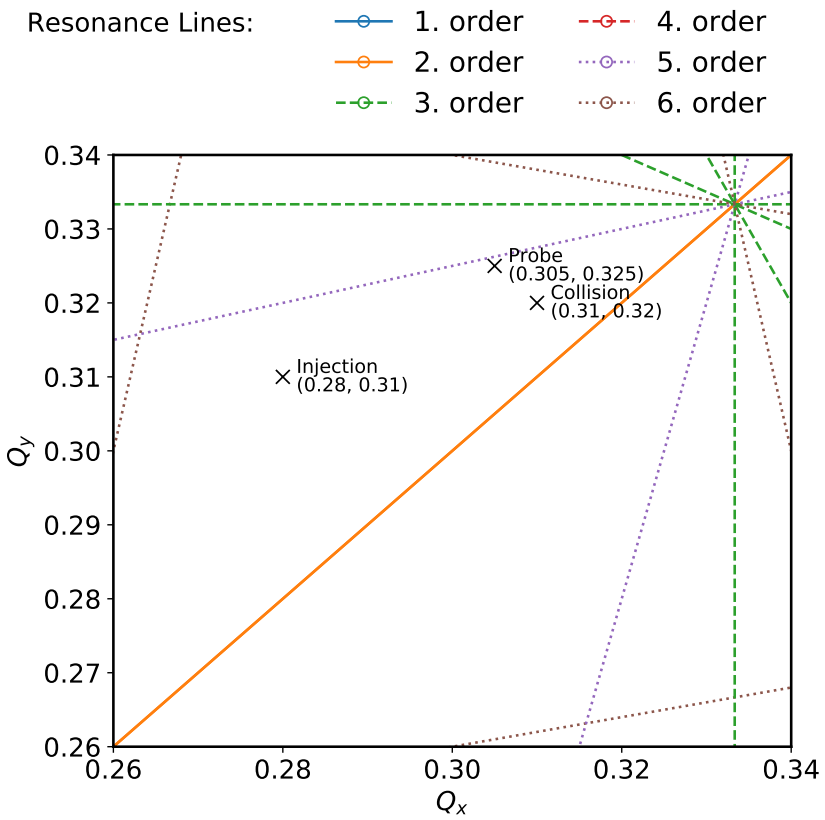

Figure 2: Tune diagram with default LHC working points at collision and injection energy as well as probed working point close to 5th order resonance line ($Q_x - 4Q_y = -1$). All resonance lines up to 6th order have been computed, but 1st and 4th order resonances are not present in the chosen window.

2.3 K-Modulation Results

The K-modulation procedure was tested during this MD to identify problems with the orbit feedback system (OFB), which was thought of as culprit for bad K-modulation measurements earlier that year. As Table 7 shows, inconsistent β^* and waist values were measured, during commissioning on the 28.04.2018, especially compared to similar measurements on the 10.04.2018.

On the 10th of april a waist-shift knob (WK), predicted to shift the Beam 1 vertical waist in IP1, had no such effect according to K-modulation results.

In the current MD the results were found to be proper and consistent.

Table 7: Results of the K-modulation measurements in IP1.
During the MD the same machine settings were used as on 28.04.2018 (see Table 3). Nominal β^* was set to 30 cm in both planes, no waist-shift applied. At full crossing, measurements were done with orbit feedback (*OFB*) on and off. On the 10.04.2018 similar settings (*Crossing**) were used, but with 145 µrad crossing angles in IP1 and IP5. A waist-shift knob for Beam 1 vertical was also applied (*WK*) and later removed (*no WK*). Also measurements at $\beta^* = 25$ cm were performed on that day.
The error given includes the fitting error, as well as a tune uncertainty of $2.5 \cdot 10^{-5}$. Misalignment, coupling, and magnetic field errors were neglected. All measurements were performed with injection tunes.

	I [A]	OFB	Config.	**Beam 1** β^* [cm] X	β^* [cm] Y	Waist [cm] X	Waist [cm] Y
10.04.2018	-	Off	Crossing*	30.0 ± 0.1	31.8 ± 0.7	3.0 ± 0.6	-7.9 ± 1.2
	-	On	Crossing*	30.02 ± 0.04	31.9 ± 0.6	-0.6 ± 0.6	-7.7 ± 1.2
	-	On	Crossing*, WK	30.08 ± 0.09	31.6 ± 0.5	2.8 ± 0.4	-7.5 ± 0.9
	-	On	Crossing*, no WK	28.98 ± 0.02	31.5 ± 0.5	-0.4 ± 0.3	-7.7 ± 0.9
	-	Off	Crossing*, β^*=25 cm	26.06 ± 0.08	29.1 ± 0.5	4.7 ± 0.2	-10.9 ± 0.5
	-	On	Crossing*, β^*=25 cm	25.30 ± 0.08	26.0 ± 0.4	1.1 ± 0.7	-6.6 ± 0.7
28.04.2018	2	On	Crossing	30.14 ± 0.06	29.5 ± 0.2	1.3 ± 0.5	-1.3 ± 1.2
	3	On	Crossing	30.09 ± 0.03	30.8 ± 0.3	1.4 ± 0.3	-6.2 ± 0.8
	3	On	Crossing	30.17 ± 0.06	32.1 ± 0.5	2.2 ± 0.4	-8.6 ± 0.7
	3.5	On	Crossing	30.30 ± 0.05	29.70 ± 0.09	2.3 ± 0.3	-1.6 ± 0.7
MD3311	5	Off	Crossing	29.81 ± 0.04	30.6 ± 0.3	2.0 ± 0.3	-6.1 ± 0.6
	5	On	Crossing	30.18 ± 0.07	31.9 ± 0.5	2.3 ± 0.4	-8.4 ± 0.8
	5	Off	Flat-Orbit	30.26 ± 0.05	30.0 ± 0.2	2.2 ± 0.3	-3.6 ± 0.6
				Beam 2 β^* [cm] X	β^* [cm] Y	Waist [cm] X	Waist [cm] Y
10.04.2018	-	Off	Crossing*	31.2 ± 0.1	30.8 ± 0.1	-2.2 ± 0.8	4.5 ± 0.5
	-	On	Crossing*	37.8 ± 2.2	30.2 ± 0.2	-14.9 ± 2.2	-2.5 ± 1.1
	-	On	Crossing*, WK	31.4 ± 0.2	31.5 ± 0.3	-3.1 ± 0.9	6.1 ± 0.8
	-	On	Crossing*, no WK	31.3 ± 0.2	30.11 ± 0.08	4.4 ± 0.6	1.7 ± 0.6
	-	Off	Crossing*, β^*=25 cm	25.88 ± 0.03	25.22 ± 0.06	0.4 ± 0.5	2.2 ± 0.3
	-	On	Crossing*, β^*=25 cm	25.6 ± 0.1	25.3 ± 0.3	-0.1 ± 1.1	3.6 ± 0.8
28.04.2018	2	On	Crossing	32.4 ± 0.6	33.0 ± 0.6	7.1 ± 1.1	9.4 ± 0.9
	3	On	Crossing	30.68 ± 0.05	30.5 ± 0.2	-0.8 ±0.6	3.5 ± 0.6
	3	On	Crossing	30.8 ± 00.1	30.6 ± 0.2	2.2± 0.8	4.2 ± 0.6
	3.5	On	Crossing	30.77 ± 0.03	30.4 ± 0.1	-0.3 ± 0.7	3.2 ± 0.6
MD3311	5	Off	Crossing	31.13 ± 0.05	30.6 ± 0.1	1.7 ± 0.4	3.4 ± 0.5
	5	On	Crossing	31.1 ± 0.1	29.96 ± 0.03	-3.5 ± 0.6	0.7 ± 0.4
	5	Off	Flat-Orbit	31.33 ± 0.09	29.98 ± 0.02	4.4 ± 0.3	-0.2 ± 0.4

2.4 Detuning Results

All amplitude detuning measurements where done using the ACD. Its influence was corrected for in the data shown, as described in [9].

Measurements with the full crossing scheme applied were done during commissioning on the 28.04.2018 (see Table 3). Measurements on flat-orbit and crossing in IP5 were done during this MD. Tune drifts are accounted for by corrections as measured by base-band tune (BBQ [31]). The BBQ is filtered and averaged as exemplarily shown in Fig. 3. The averaging algorithm is as follows: First, all data outside of a rough cut around the expected tune, usually $0.5 \cdot 10^{-3}$ to 10^{-3}, is discarded, to not include the ACD kicks in the averaging. Then a rough averaging, using a moving average window of 200-1000 samples, is performed. To eliminate noise outliers, a second cut of 10^{-4} around this average is applied on all samples and the remaining data is then again averaged by a moving average of window-length 100.

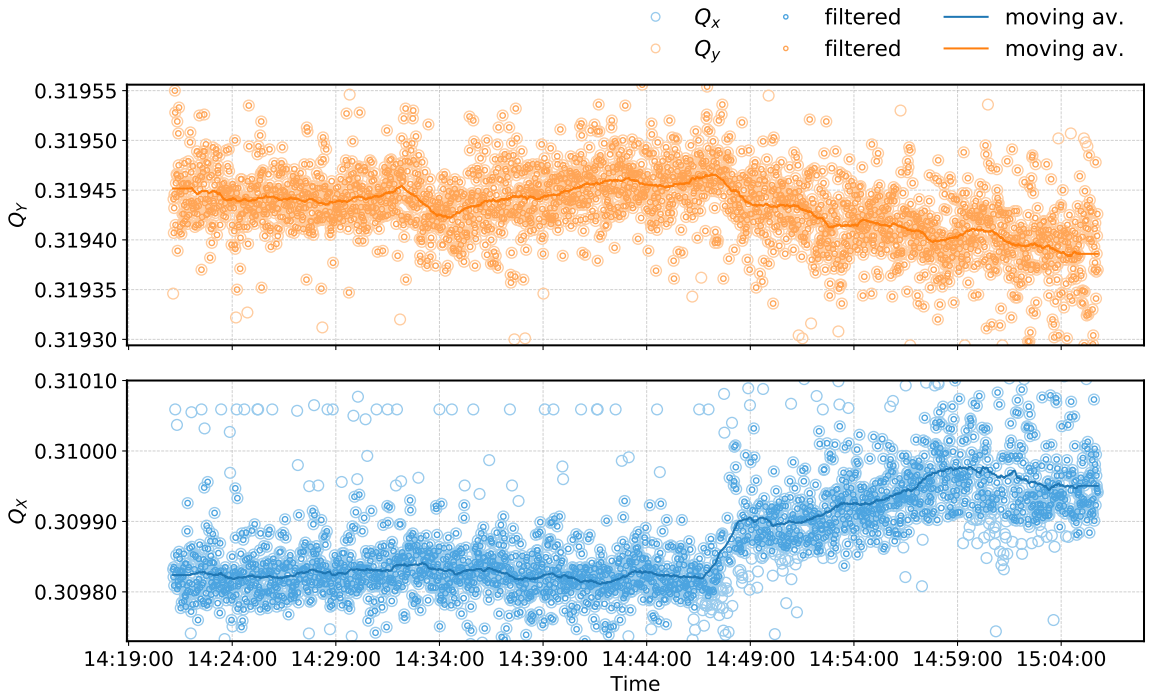

Figure 3: BBQ measurement. Shown here as an example is the tune from Beam 2 during horizontal kicks with full crossing from commissioning. The data is filtered with a rough-cut of 10^{-3} around $Q_x = 0.31$ and $Q_y = 0.32$ first and, after applying a moving average of window-length 200, a second cut of 10^{-4} is applied. The remaining data-points (labled "filtered") contribute to the final moving average of window-length 100, which is then used for tune-drift correction.

Figures 4 and 5 show the comparison between the MD measurements for flat-orbit and IP5 crossing and also commissioning data at full crossing scheme. While the flat-orbit configuration seen in Fig. 4a exhibits only a negligible amount of detuning, enabling crossing in IP5 leads to a detuning even stronger than detuning at commissioning. Consequently, this indicates the presence of decapole or dodecapole field errors in IP5 which lead to feed-

down to amplitude detuning upon horizontal orbit deviations. An extensive investigation of sources of detuning is done by means of simulations in Section 3. It can be seen from Fig. 6 that with the applied crossing scheme, orbit deviations in both planes are present in IP5. Therefore, both, skew and normal, field-error components are contributing to feed-down.

The horizontal cross-term in Beam 1, seen in Fig. 4b, shows little variation between flat-orbit and crossing angles: The measurement for the IP5 crossing configuration was very noisy and should only be considered with caution. Small positive detuning coefficients are seen for the other two measurements.

Unfortunately, too much noise on the MD measurement prohibited a meaningful analysis of the vertical plane cross-term in the same beam (Fig. 4c). Only the data from commissioning yields reasonable results, which are higher than for the $\partial Q_y/\partial(2J_x)$ cross-term, but of comparable order.

Flat-orbit and IP5-crossing configurations show almost no detuning present for the beam 1 direct vertical term (Fig. 4d), yet a strong negative detuning is present for the full crossing scheme. It seems to stem from IP1 then, but there is no data available to verify this assumption.

For Beam 2, the observed behavior of the direct horizontal term is shown in Fig. 5a: a small negative detuning can be seen in the flat-orbit case, an even smaller for the full crossing scheme and almost zero detuning is present with IP5 crossing angles.

The cross-terms for Beam 2 in Figs. 5b and 5c show small detuning for this beam for the MD measurements and no detuning for the full crossing scheme for $\partial Q_y/\partial(2J_x)$. The full-crossing measurement of $\partial Q_x/\partial(2J_y)$ should be regarded as too noisy to provide valuable insight.

While there is some detuning visible for the vertical direct term shown in Fig. 5d, which increases when enabling crossing in IP5, it is only about a third of the $\partial Q_x/\partial(2J_x)$ term in Beam 1 or the $\partial Q_y/\partial(2J_y)$ full crossing scenario of the same beam. IP5 crossing and full crossing configurations agree very well, even though only the low-amplitude kicks could be taken into account in the latter case due to a noise-line emerging at higher amplitudes. Detuning for flat-orbit is about half the value of the crossing configurations.

Both Beam 2 direct term measurements at flat-orbit indicate, that the octupolar magnetic field errors are not as well corrected as they were in 2017, when they where only a third of their current value ($\partial Q_x/\partial(2J_x)$ is $(-7 \pm 1) \cdot 10^3\,\mathrm{m}^{-1}$, was $(-2 \pm 1) \cdot 10^3\,\mathrm{m}^{-1}$ and $\partial Q_y/\partial(2J_y)$ is $(6 \pm 1) \cdot 10^3\,\mathrm{m}^{-1}$, was $(2 \pm 1) \cdot 10^3\,\mathrm{m}^{-1}$; see Table 2).

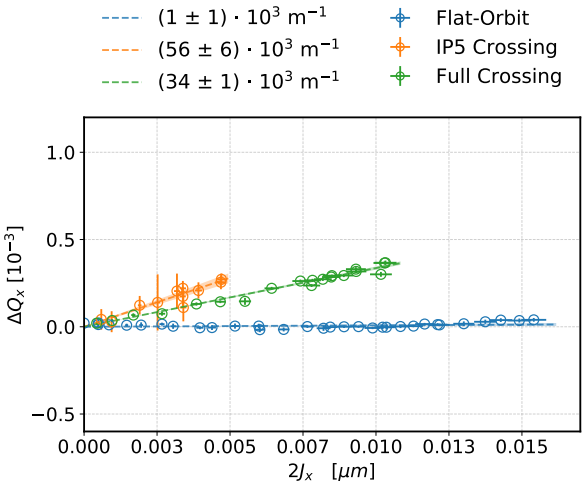

(a) Beam 1 $\partial Q_x/\partial(2J_x)$

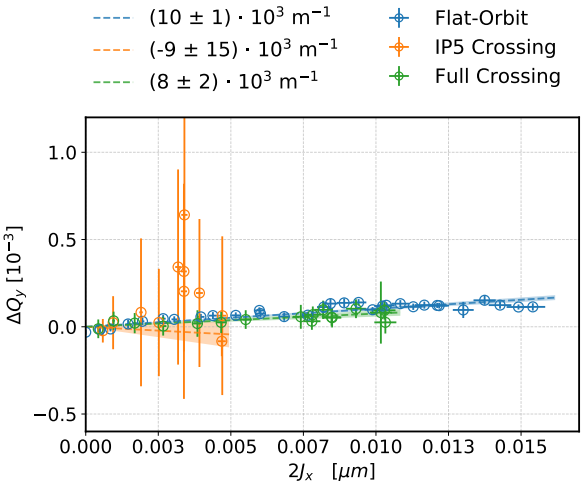

(b) Beam 1 $\partial Q_y/\partial(2J_x)$

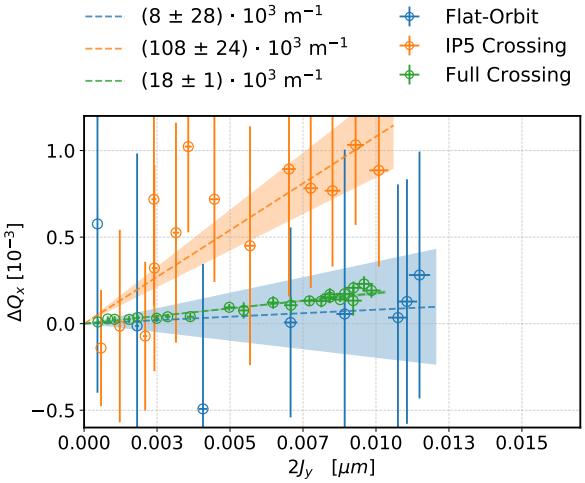

(c) Beam 1 $\partial Q_x/\partial(2J_y)$

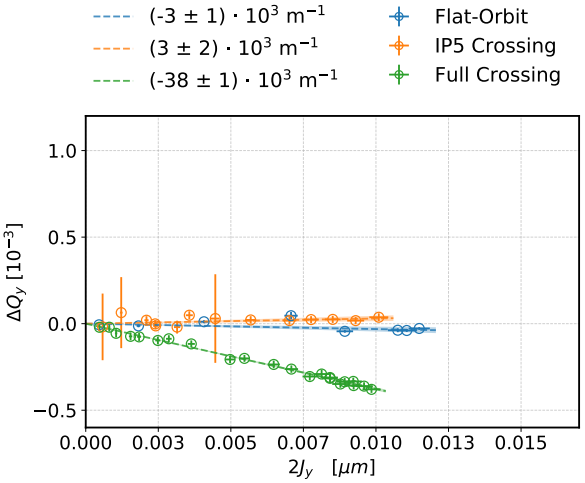

(d) Beam 1 $\partial Q_y/\partial(2J_y)$

Figure 4: Detuning with amplitude in Beam 1. Comparison between commissioning (full crossing) and results from MD3311 (flat-orbit and crossing in IP5). Horizontal kicks are shown in the top charts, vertical kicks at the bottom. The dashed lines and colored area represent the respective fit and one standard deviation fitting error. Their values are given in the legend.

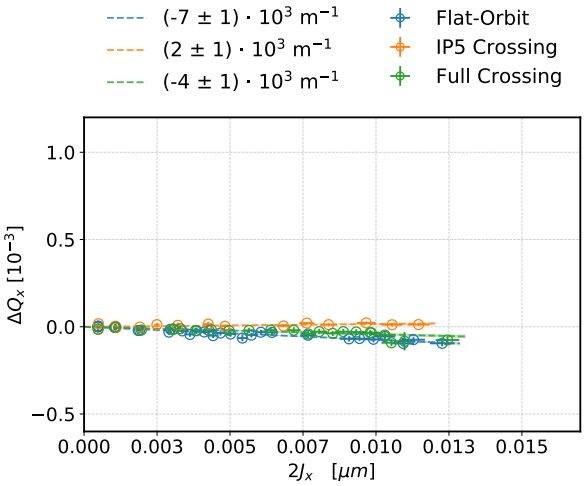

(a) Beam 2 $\partial Q_x/\partial(2J_x)$

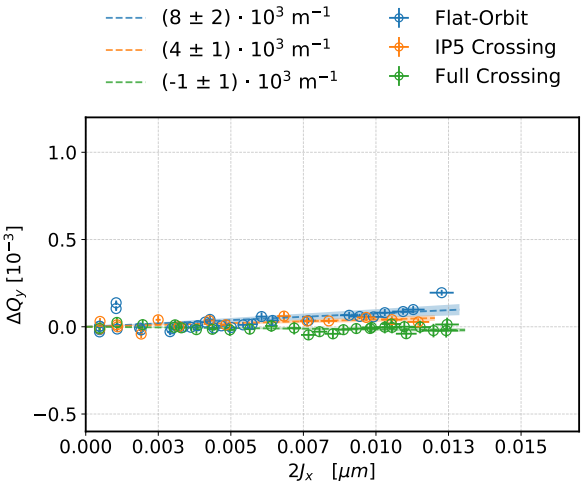

(b) Beam 2 $\partial Q_y/\partial(2J_x)$

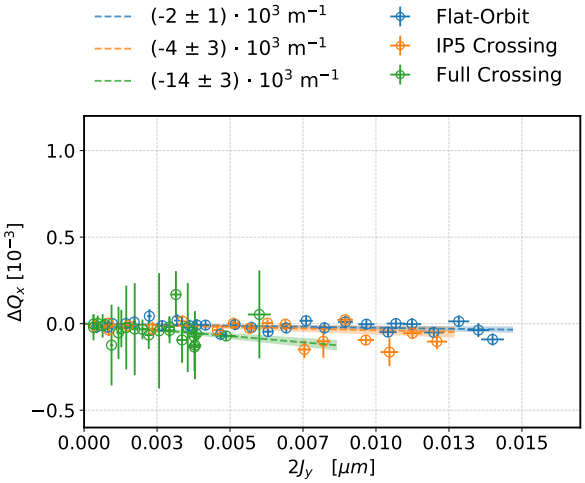

(c) Beam 2 $\partial Q_x/\partial(2J_y)$

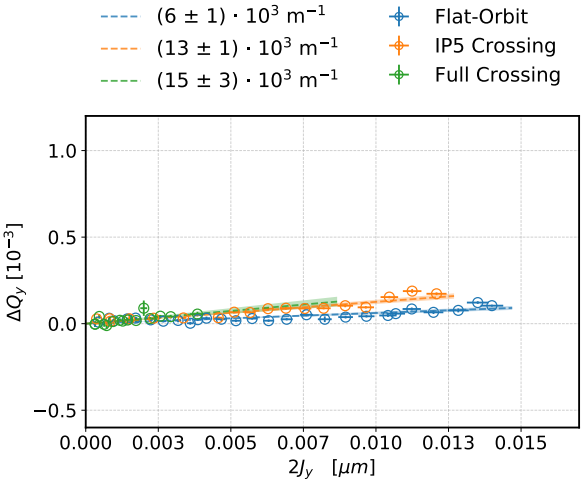

(d) Beam 2 $\partial Q_y/\partial(2J_y)$

Figure 5: Detuning with amplitude in Beam 2. Comparison between commissioning (full crossing) and results from MD3311 (flat-orbit and crossing in IP5). Horizontal kicks are shown in the top charts, vertical kicks at the bottom. The dashed lines and colored area represent the respective fit and one standard deviation fitting error. Their values are given in the legend.

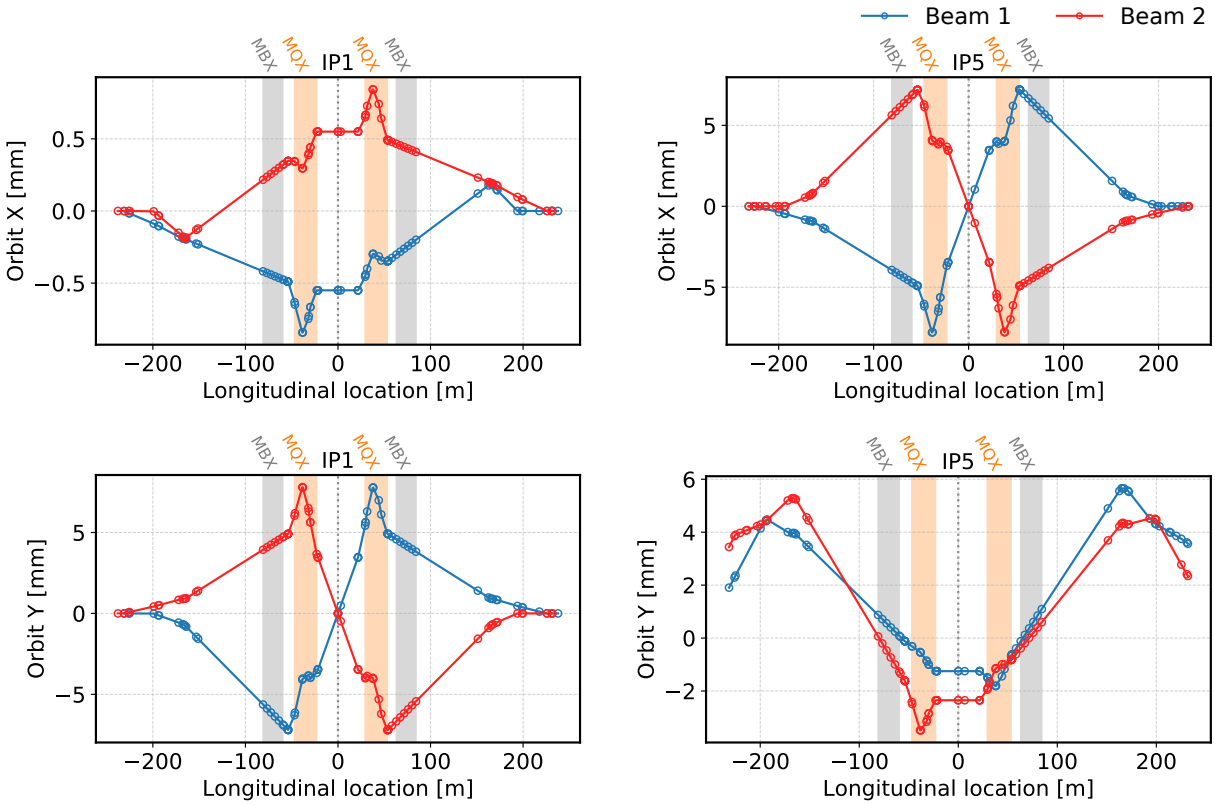

Figure 6: Simulated orbit around IP1 and IP5 for both beams. Simulation settings as given in Table 8. Locations of the MQX are marked in orange, locations of the MBXW in grey.

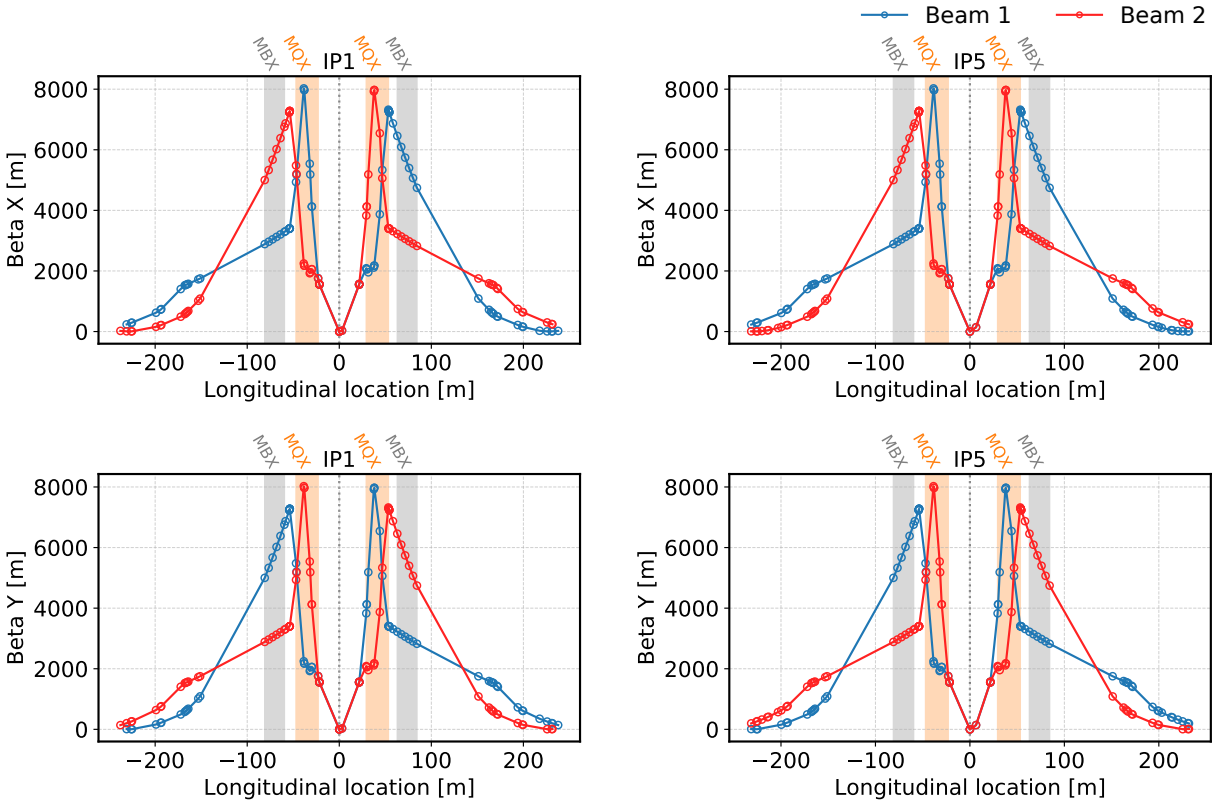

Figure 7: Simulated β-function around IP1 and IP5 for both beams. Simulation settings as given in Table 8. Locations of the MQX are marked in orange, locations of the MBXW in grey.

3 Simulations

3.1 Simulation Setup

Table 8: Simulation settings. Signs as set in MAD-X. Set to be close to measurement settings, see Tables 3 and 4.

Tunes		Q_x 0.31	Q_y 0.32
		IP1	IP5
β^*	[cm]	30	30
Crossing Angle	[µrad]	160	160
Separation	[mm]	-0.55	0.55
Offset	[mm]	0	-1.8

Table 9: Approximate orbit values in the MQX due to orbit settings in the IP as seen in Table 8 (signs for Beam 1 left / right magnets). Visualisation in Fig. 6.

		IP1	IP5
Δx	[mm]	(–/–) $0.3 - 0.8$	(–/+) $4 - 8$
Δy	[mm]	(–/+) $3 - 8$	(–/–) $1 - 3$

To identify possible sources of amplitude detuning in the presence of crossing angles, simulations were run, modeling the machine status, see Table 8. The measurements shown in Section 2.4 indicate the detuning origin from feed-down in either IP1 or IP5, therefore crossing-angles were applied in these IPs individually as well as combined. As expected from measurements, the simulations do not show second-order effects of the magnetic field strength on amplitude detuning, leaving the contributions from the IPs independent of each other. Simulations show (see Appendix B), that the amplitude detuning created by $(b_3)^2$ is about an order of magnitude smaller than the amplitude detuning direct terms created by b_4 (Fig. 10). Feed-down to b_3 is expected to be even weaker, which is in agreement with the experience from measurements: the sextupole correction has changed over the years, while the amplitude detuning changed only by small amounts (e.g. flat-orbit entries from 2016, 2017 and 2018 in Table 2).

In conclusion, b_4 and feed-down to b_4 dominate the amplitude detuning seen. In Table 9 and Figs. 6 and 7 the consequences of these settings on the orbit and β-function in the MQX are summarized.

Magnetic field multipole errors of different orders are used in the model, namely: normal octupoles (b_4), normal and skew decapoles (b_5 and a_5) and normal and skew dodecapoles (b_6 and a_6). These errors are provided from WISE [14] models. The uncertainties in the errors are taken care of by usage of the 60 seeds for 6.5 TeV and 40 cm optics, which can be found

in [32]. Shown are the mean value of the simulation results over these seeds with errorbars given by the standard deviation.

It should be noted here, that error values b_4 of the MQXB and the error values a_6 of the MQXA do not change over the range of all WISE seeds. Further, the WISE tables used contain only b_5 errors for MBXW magnets. The distributions are shown in Appendix A.

Amplitude detuning is calculated at different stages during the simulation with the ptc_normal module [33]. Before each stage, the tunes are matched to their original values.

3.2 Simulation Results

The results of the simulations described in Section 3.1 are shown in Figs. 10 to 16. Sections 3.2.1 to 3.2.5 investigate the influence of b_4, b_5, a_5,b_6 and a_6, on detuning independently, while Section 3.2.6 shows their combined effect. In Section 3.2.7 only the decapolar and dodecapolar field errors are under test. This configuration represents perfect b_4 correction in the machine. As b_4 is assumed to be well corrected in the current machine [20, 21], these settings represent closely the state of the machine during measurement and measurement data is shown for comparison.

The different output stages, at which detuning is calculated, are:

- **Nominal:** Before applying any errors.
- **Arc errors:** Errors applied in the arcs (M[B,Q] of the arcs)
- **MQX errors:** *Arc Errors* and errors in the MQX (MQX)
- **Sep. MB errors:** *All errors above* and errors in the separation dipoles (MB[XW,RC,X,RB,RS,W])
- **All errors:** *All errors above* and remaining MQ-errors (MQ[Y,M,MC,ML,TL,W])
- **Corrected:** *All errors above* and nominal Triplet and D1 correction applied.

The *'corrected'* stage shows the best correction possible using the correctors, common to both beams, in the IP [28].

3.2.1 b_4 Errors

As first-order amplitude detuning ($\propto$J) is created in first order by normal octupole field components [3, 4, 9], the normal octuple field errors contribute directly, while higher order multipoles are contributing via feed-down to b_4 [1]. Consequently no orbit offset is required and, in contrast to the other multipole errors, detuning is present even for flat-orbit, as seen in Fig. 10. In fact, the detuning does not change with crossing angles for Beam 1 at all, and there is only a slight difference for Beam 2. Also in consequence, amplitude-dependent

[1] While this statement is technically not true for normal dodecapoles, as they contribute directly to second order amplitude detuning ($\propto J^2$), this contribution is currently assumed to be negligible in the LHC. See Section 3.2.4.

detuning caused by b_4 is larger than for any other error - about twice of the maximum value of any other component, as seen in the following sections. As normal octupole correctors are present in the IPs [28], the detuning, though large, can be well mitigated.

The detuning of the measurements varies with crossing scheme, so b_4 cannot be responsible for the experimentally found detuning changes.

3.2.2 b_5 Errors

Normal decapole field errors feed down to b_4 via Δx [13]. According to Table 9 the contribution from IP1 should be therefore an order of magnitude less, than from IP5 (assuming similar error strengths in the two IPs, see Appendix A, and β-function, see Fig. 7). This can be observed in Fig. 11: The flat-orbit and IP1 crossing configurations show no and very small detuning, respectively. Activating crossing in IP5 yields strong detuning, especially in the direct horizontal term (Fig. 11a) and cross term (Fig. 11e) in Beam 1, as well as the direct vertical term in Beam 2 (Fig. 11d). The strength is between a third and half of the strength from b_4 errors. As the contribution from IP1 crossing is small, the curve of combined crossing angles is almost identical to the curve with IP5 crossing only.

A small but noticeable change in detuning can be observed, when adding the field errors to the IP-dipoles in IP5. As b_5 is the only field-error order given in the WISE tables for the MBXW (see Appendix A), the other orders do not show this behaviour.

3.2.3 a_5 Errors

Skew decapole field errors feed down to b_4 via Δy and hence show a great dependency on IP1 crossing and less so on IP5 crossing, visible in the direct terms of Beam 1 (Figs. 12a and 12c) and in the vertical direct term and cross term of Beam 2 (Figs. 12d and 12f). The cross term of Beam 1 on the other hand is dominated by IP5 (Fig. 12e), and the horizontal direct term of Beam 2 shows almost equal contributions from IP1 an IP5, but with opposite sign, leading to a detuning compensation, when both crossing angles are active (Fig. 12b).

3.2.4 b_6 Errors

Normal dodecapole errors feed down to b_4 via Δx^2 and $-\Delta y^2$, therefore crossing in either IP causes detuning. In Beam 1 detuning of similar order of magnitude, but with different signs, is present for both IP crossings in all terms (Figs. 13a, 13c and 13e). In Beam 2 on the other hand, the detuning is much stronger, but only present for IP5 crossing in the horizontal term (Fig. 13b) and only for IP1 crossing in the vertical term (Fig. 13d), while equally strong for both IPs in the crossing term (Fig. 13f).

As the flat orbit detuning does not change visibly after adding the field errors to the simulation, and because the contributions from the IPs are independent and add up very well when both activated, contribution from b_6 to second order detuning is shown to be negligible.

3.2.5 a_6 Errors

The feed-down from skew dodecapole errors is proportional to the product $\Delta x \Delta y$ and leads to strong amplitude detuning with IP5 crossing in all terms but the vertical direct term of Beam 1, where no detuning is observed (Fig. 14). IP1 does not contribute significantly and hence the curves for the combined crossing scheme follows that of IP5 very closely.

3.2.6 b_4, b_5, a_5, b_6, a_6 Errors

Applying all multipole errors at the same time shows the direct terms to be dominated by the b_4 components (Fig. 15). Yet, in the case of Beam 1 direct horizontal detuning, the detuning with IP5 crossing is almost doubled, compared to the same b_4 detuning term, while it stays about the same for IP1. This shows already, that in this case the contributions from the individual field errors above b_4 cancel in IP1, while they enhance each other in IP5. The opposite is true in the case of direct vertical detuning in Beam 2, where contributions from feed-down in IP1 lead to a reduction in detuning compared to the flat-orbit case. These traits can be observed more clearly in Section 3.2.7.

3.2.7 b_5, a_5, b_6, a_6 Errors

Deactivating the contribution from b_4 models the case of perfect b_4 correction in the machine and should be the closest to the machine state during MD3311 measurements. Simulation and measurement results can be seen in Fig. 16.

All detuning contributions come from feed-down, which is obvious from the unchanging flat-orbit case. The direct terms are dominated by contributions from IP5 crossing (Figs. 16a to 16c), apart from the vertical term in Beam 2, where IP1 is the dominant influence (Fig. 16d).

Measurement and simulation are not in stark disagreement and show at least detuning values of similar magnitude. Figure 8 shows the change in amplitude detuning between the IP5 crossing and flat-orbit, for the measurement from MD3311 as well as for the current simulation setting and when all errors are applied. As there is agreement for only two data points, there are obviously effects influencing amplitude detuning through crossing angles not yet accounted for.

3.2.8 Coupling

Linear coupling was checked at the end of the simulations, as it influences the detuning coefficients [18], using closest tune approach [34]: Matching the fractional tunes as close as possible (i.e. for collision tunes $Q_x = 62.315$ and $Q_y = 60.315$), the remaining ΔQ_{min} equals the global measure $|C^-|$ for coupling, which is generated by the difference driving term f_{1001} [2], which in turn is generated by skew quadrupolar magnetic field errors a_2 [35]. As seen in Fig. 9 no coupling is present for flat orbit, but feed-down creates coupling in the machine, especially from b_4 and b_6 magnetic field errors. b_5, a_5 and a_6 cause $|C^-| < 10^{-6}$ in the simulations and are not shown here. Also not shown is the coupling result from the simulation with combined b_5, a_5, b_6 and a_6 errors applied, as with the b_6 contribution being two orders above the others, the distribution looks identical to the result from b_6 alone.

Coupling is dominated by feed-down in IP5 and contribution from b_4 is 4-5 times stronger than from b_6. Also, coupling from IP5 in Beam 2 is about 3 times larger than in Beam 1.

Yet, even the highest values, for Beam 2 with IP1 and IP5 crossing active, coupling is an order of magnitude smaller, than the strong coupling case in [18] of $|C^-| = 2 \cdot 10^{-2}$. All other values are below of what is considered very well corrected coupling $|C^-| < 10^{-3}|$ in [18, 36]. It follows, that coupling should not influence the simulated detuning results.

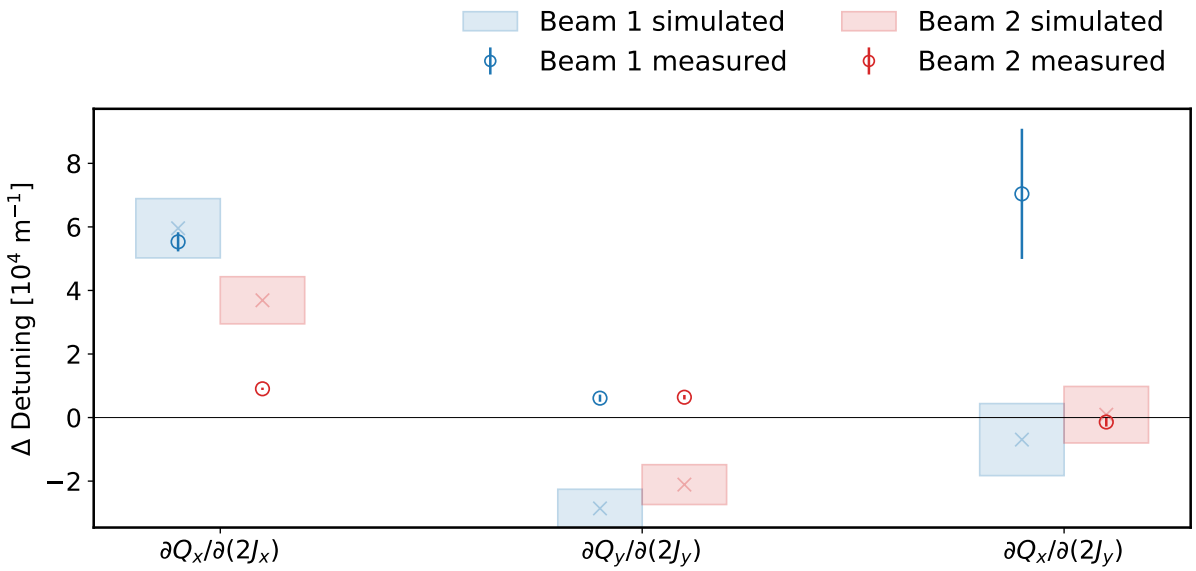

Figure 8: Change in amplitude detuning from flat-orbit to the IP5 crossing scheme. Comparison between measurement from MD3311 and simulation with b_5, a_5, b_6 and a_6 magnetic field-errors applied, before the triplet-correction was conducted. This is the **difference** of the data seen in Fig. 16 at the *'errors all'* stage between the *'IP5 crossing'* and *'Flat-Orbit'* line.

3.2.9 Summary

Sections 3.2.1 to 3.2.7 show that the biggest contribution to first-order amplitude detuning from all multipole sources stem from the MQX. This is not surprising, as the β-function, influencing the detuning quadratically, reaches values of up to 8 km (Fig. 7) in these magnets. The other IP magnets seem to play a smaller yet still significant role for amplitude detuning due to feed-down from b_5. Contribution of arc magnets are small for all investigated cases. Responsible for the largest detuning is b_4, yet also b_5 and b_6 can cause detuning up to half of b_4, each. Apart from these main contributors, the other multipole errors under test show small but non-negligible contribution to detuning as well.

Simulations with all errors and all decapolar and dodecapolar errors applied, as done in Sections 3.2.6 and 3.2.7, show a complex detuning behavior. While the results are comparable to the measurements in strength, they do not agree in most cases.

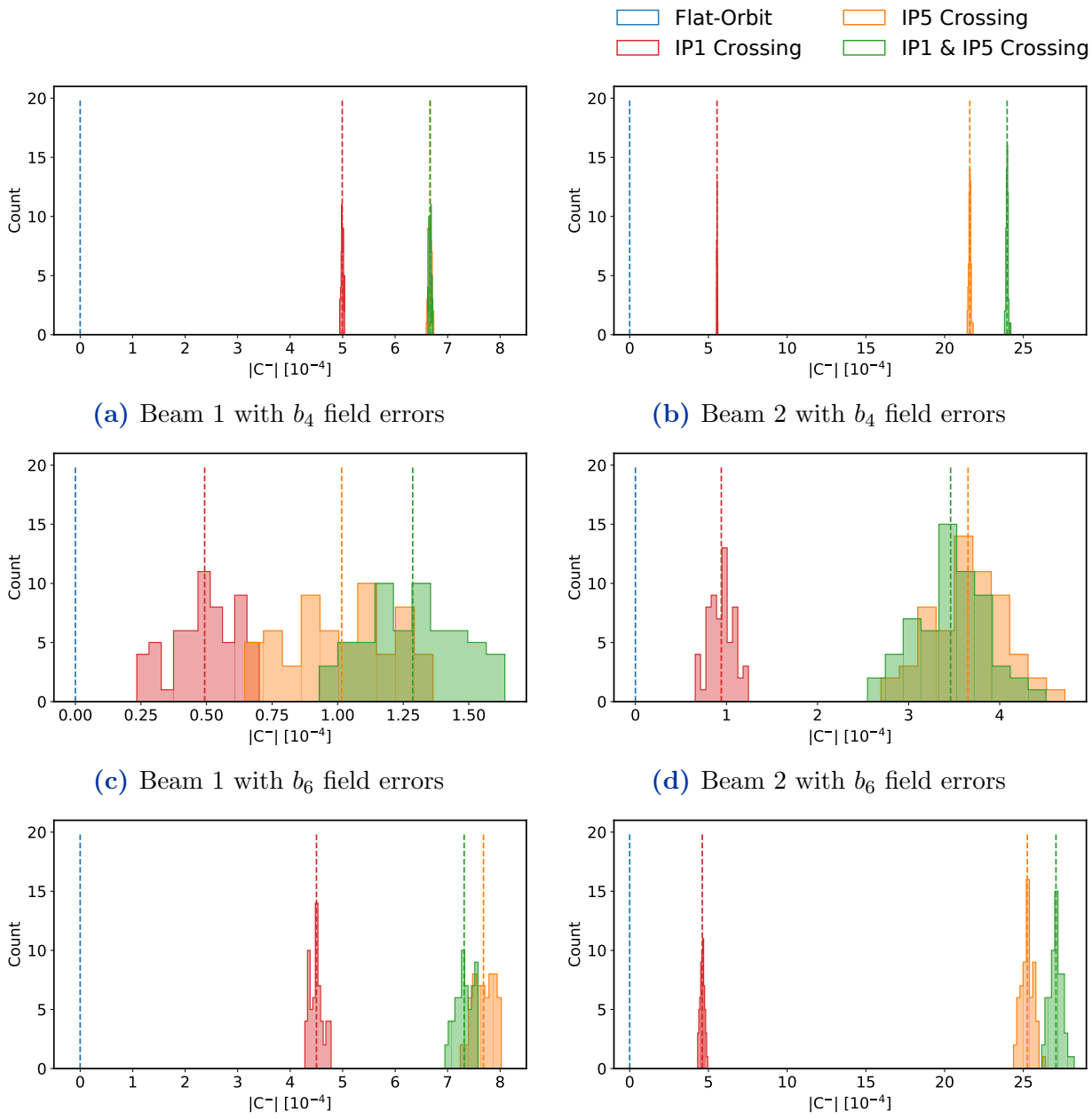

(a) Beam 1 with b_4 field errors

(b) Beam 2 with b_4 field errors

(c) Beam 1 with b_6 field errors

(d) Beam 2 with b_6 field errors

(e) Beam 1 with b_4, b_5, a_5, b_6 and a_6 field errors

(f) Beam 2 with b_4, b_5, a_5, b_6 and a_6 field errors

Figure 9: Coupling distribution at the end of the simulations for Beam 1 (left column) and Beam 2 (right column). The histogram shows the distribution over the WISE seeds, the dashed line its mean value.

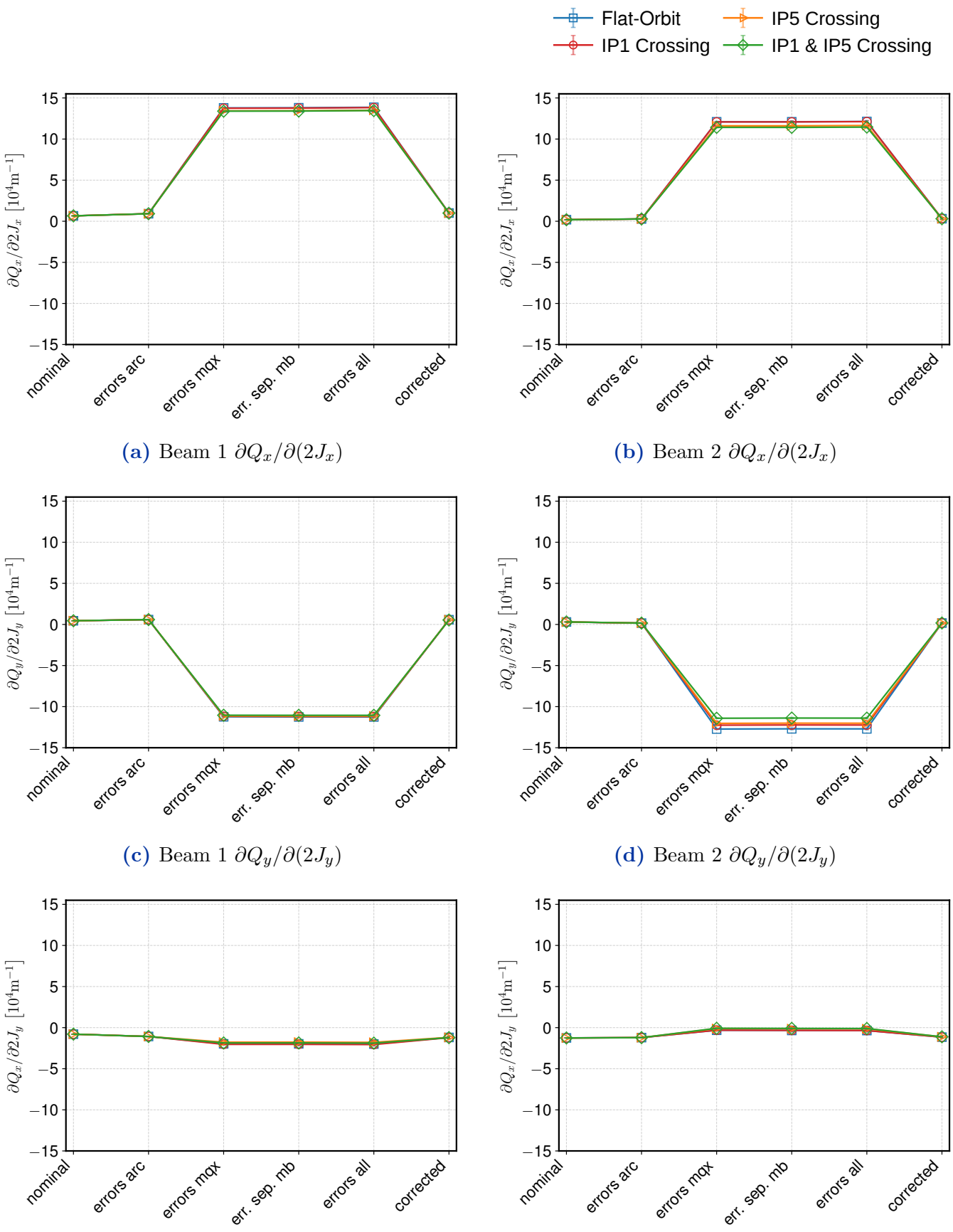

(a) Beam 1 $\partial Q_x/\partial(2J_x)$

(b) Beam 2 $\partial Q_x/\partial(2J_x)$

(c) Beam 1 $\partial Q_y/\partial(2J_y)$

(d) Beam 2 $\partial Q_y/\partial(2J_y)$

(e) Beam 1 $\partial Q_x/\partial(2J_y)$

(f) Beam 2 $\partial Q_x/\partial(2J_y)$

Figure 10: Simulation results with only b_4 errors.

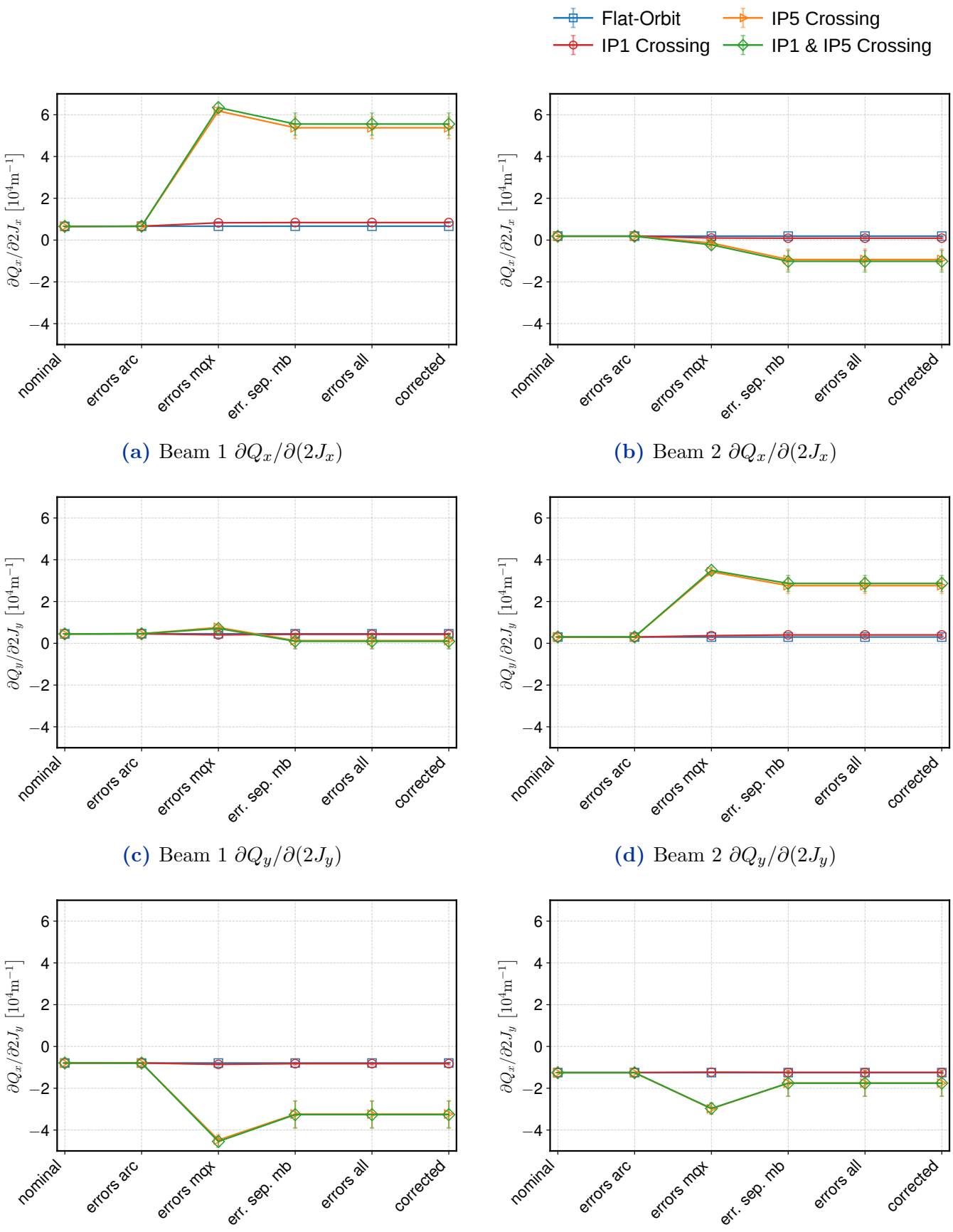

(a) Beam 1 $\partial Q_x/\partial(2J_x)$

(b) Beam 2 $\partial Q_x/\partial(2J_x)$

(c) Beam 1 $\partial Q_y/\partial(2J_y)$

(d) Beam 2 $\partial Q_y/\partial(2J_y)$

(e) Beam 1 $\partial Q_x/\partial(2J_y)$

(f) Beam 2 $\partial Q_x/\partial(2J_y)$

Figure 11: Simulation results with only b_5 errors.

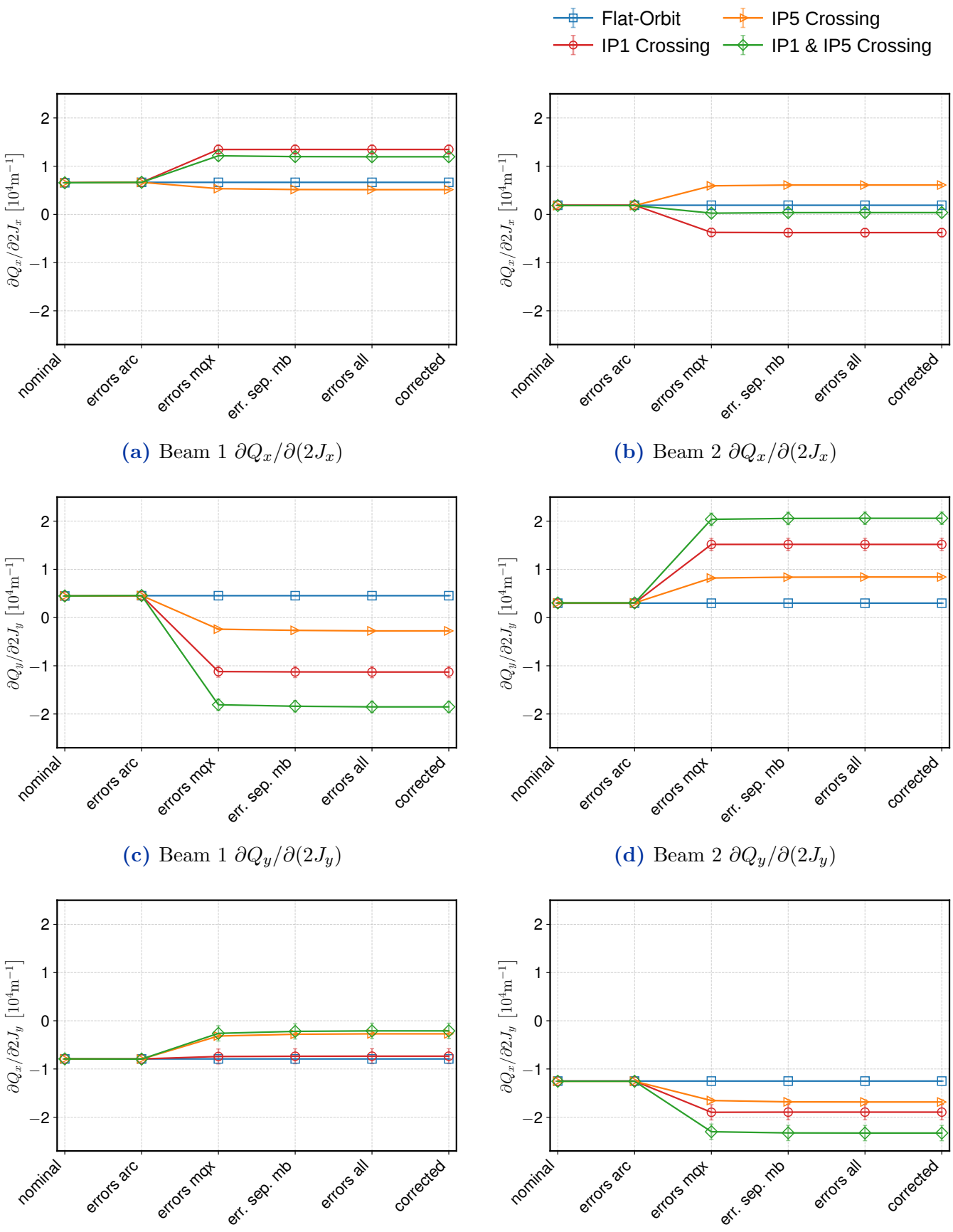

(a) Beam 1 $\partial Q_x/\partial(2J_x)$

(b) Beam 2 $\partial Q_x/\partial(2J_x)$

(c) Beam 1 $\partial Q_y/\partial(2J_y)$

(d) Beam 2 $\partial Q_y/\partial(2J_y)$

(e) Beam 1 $\partial Q_x/\partial(2J_y)$

(f) Beam 2 $\partial Q_x/\partial(2J_y)$

Figure 12: Simulation results with only a_5 errors.

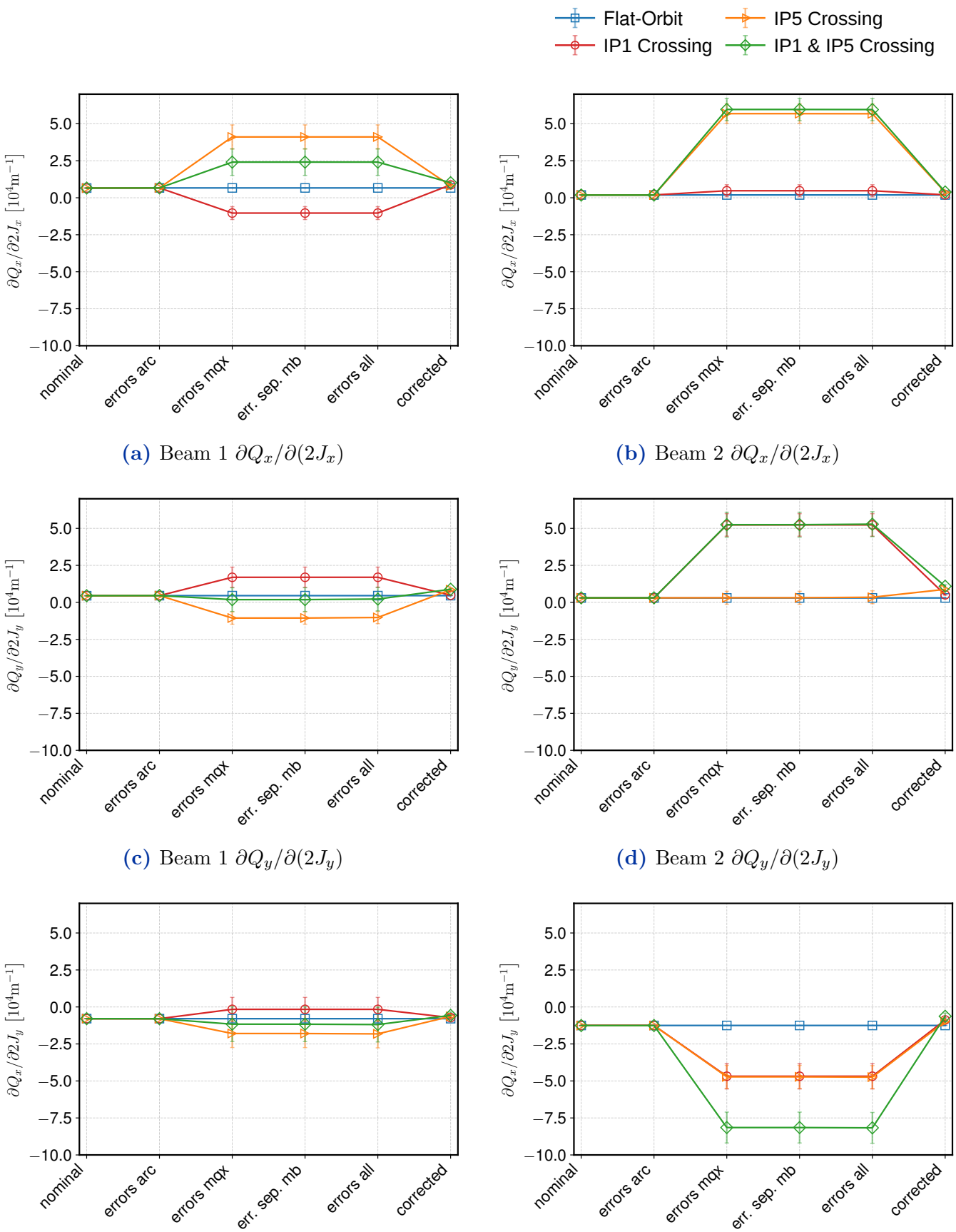

(a) Beam 1 $\partial Q_x/\partial(2J_x)$

(b) Beam 2 $\partial Q_x/\partial(2J_x)$

(c) Beam 1 $\partial Q_y/\partial(2J_y)$

(d) Beam 2 $\partial Q_y/\partial(2J_y)$

(e) Beam 1 $\partial Q_x/\partial(2J_y)$

(f) Beam 2 $\partial Q_x/\partial(2J_y)$

Figure 13: Simulation results with only b_6 errors.

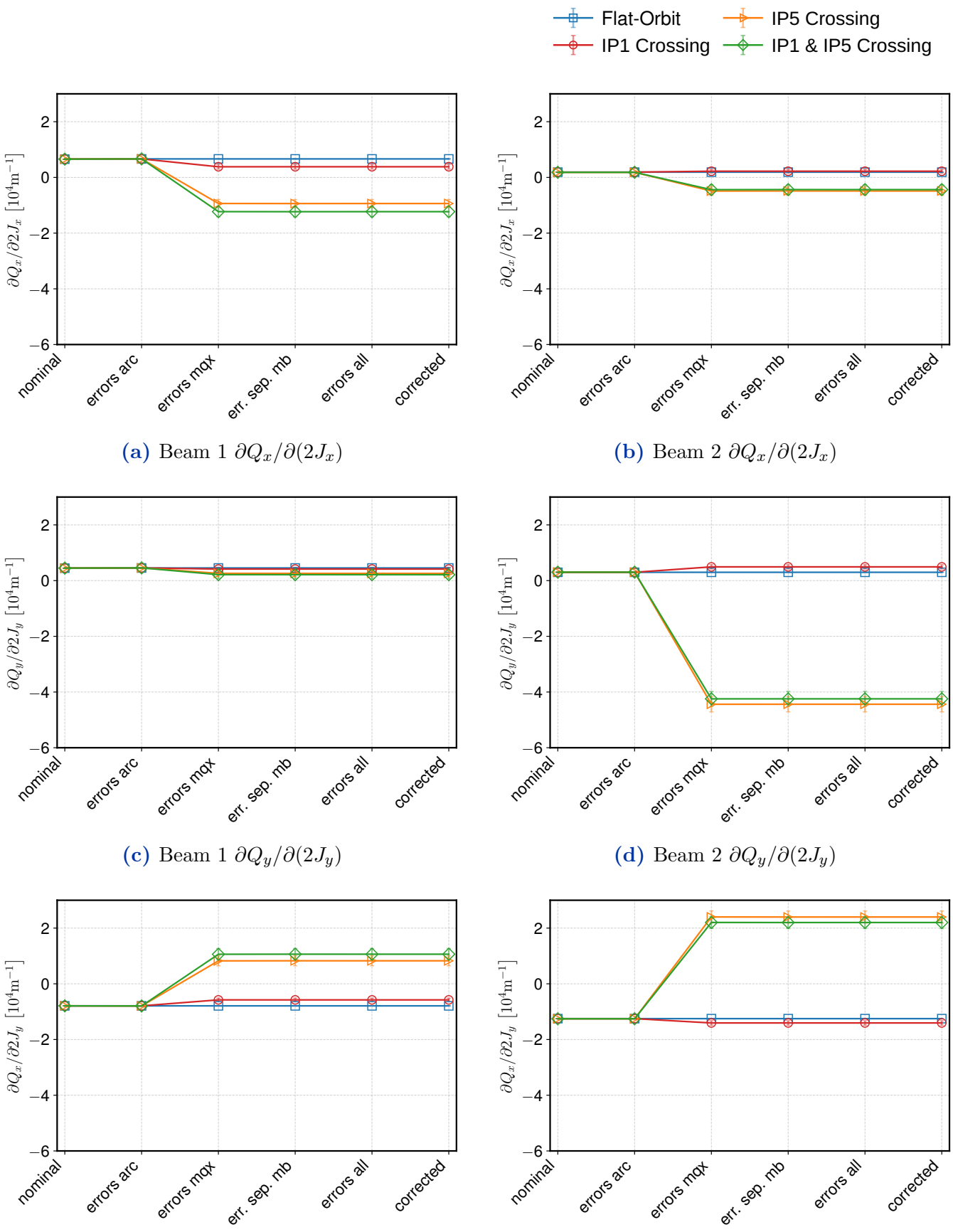

(a) Beam 1 $\partial Q_x/\partial(2J_x)$

(b) Beam 2 $\partial Q_x/\partial(2J_x)$

(c) Beam 1 $\partial Q_y/\partial(2J_y)$

(d) Beam 2 $\partial Q_y/\partial(2J_y)$

(e) Beam 1 $\partial Q_x/\partial(2J_y)$

(f) Beam 2 $\partial Q_x/\partial(2J_y)$

Figure 14: Simulation results with only a_6 errors.

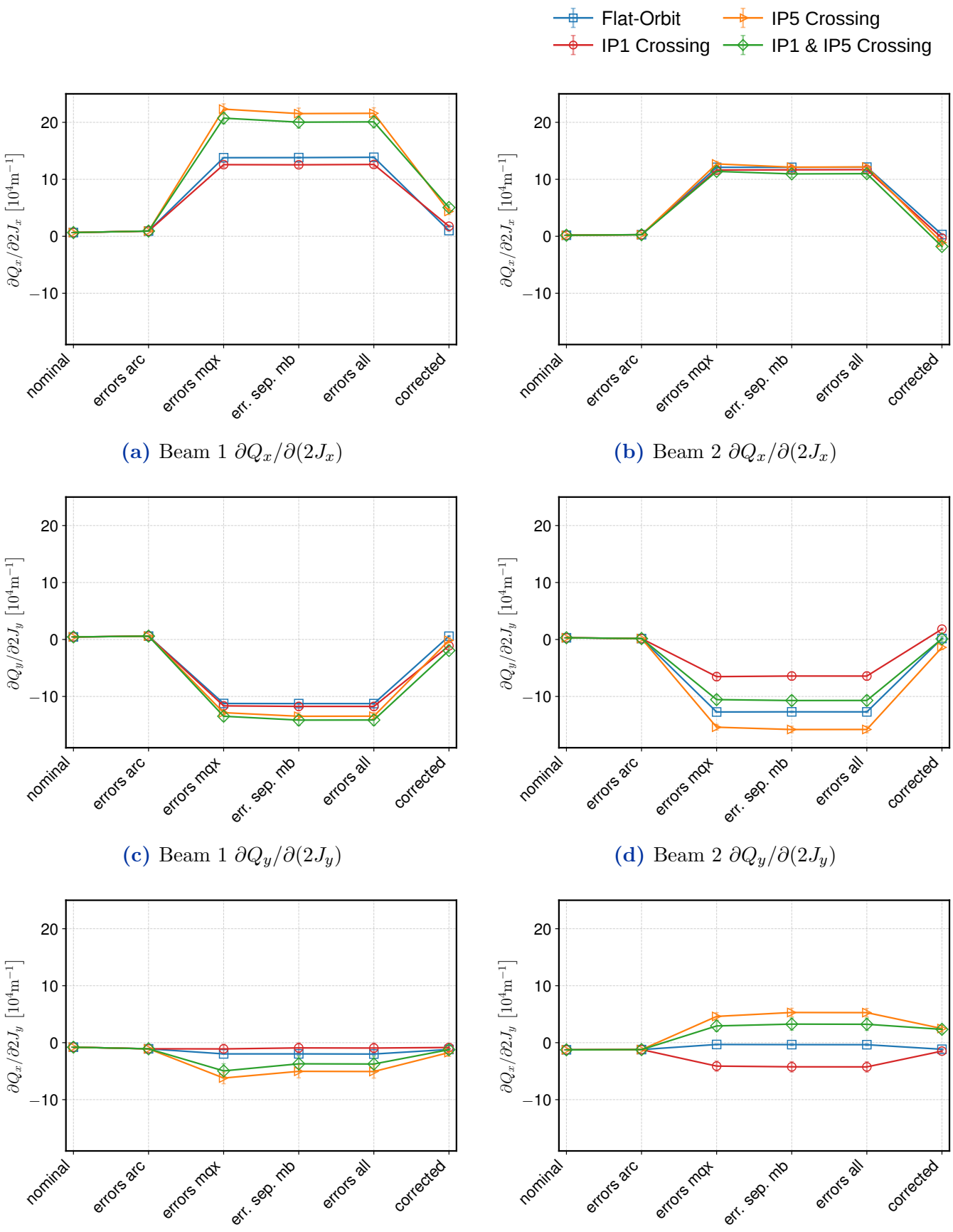

(a) Beam 1 $\partial Q_x/\partial(2J_x)$

(b) Beam 2 $\partial Q_x/\partial(2J_x)$

(c) Beam 1 $\partial Q_y/\partial(2J_y)$

(d) Beam 2 $\partial Q_y/\partial(2J_y)$

(e) Beam 1 $\partial Q_x/\partial(2J_y)$

(f) Beam 2 $\partial Q_x/\partial(2J_y)$

Figure 15: Simulation results with b_4, b_5, a_5, b_6 and a_6 errors.

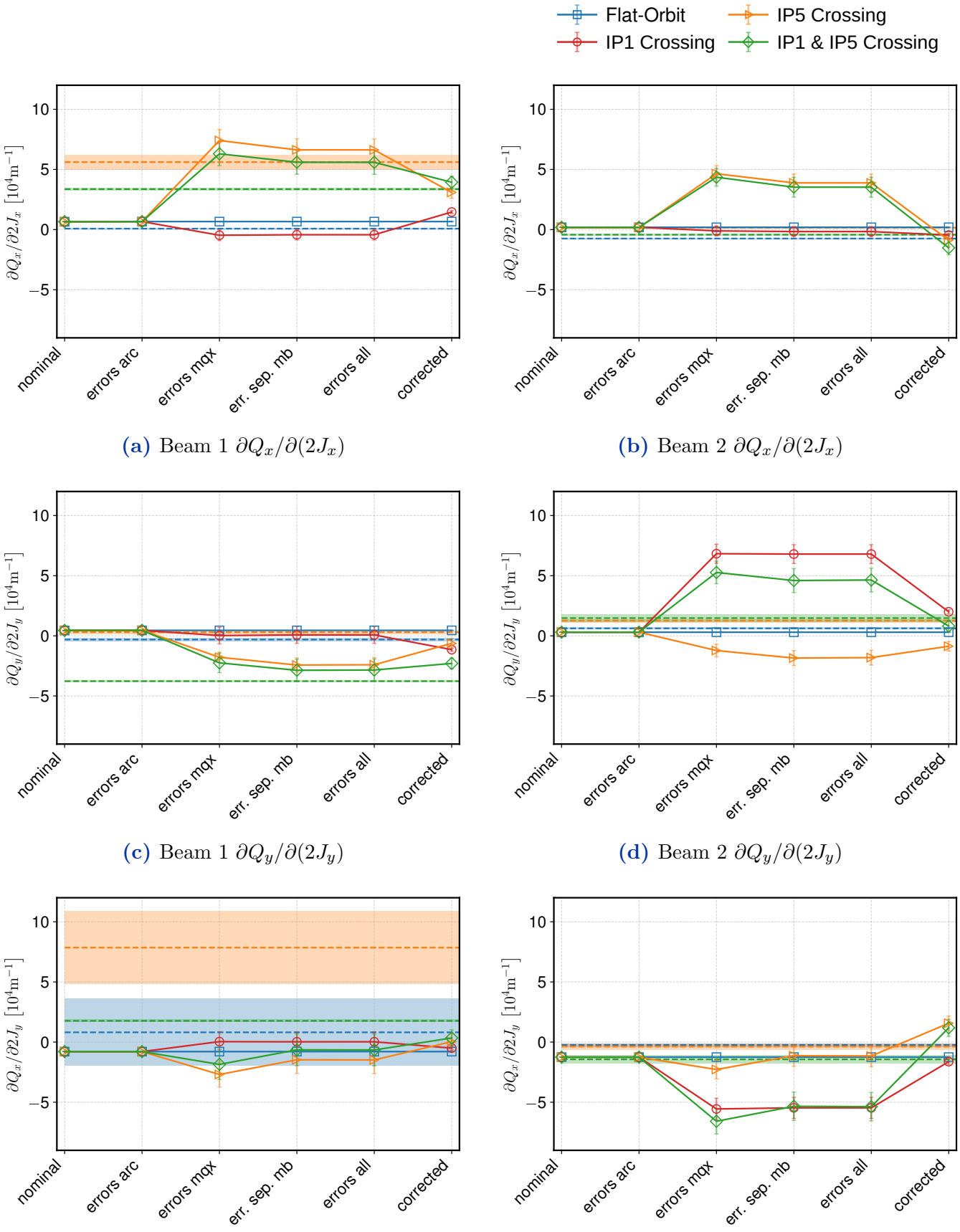

(a) Beam 1 $\partial Q_x/\partial(2J_x)$

(b) Beam 2 $\partial Q_x/\partial(2J_x)$

(c) Beam 1 $\partial Q_y/\partial(2J_y)$

(d) Beam 2 $\partial Q_y/\partial(2J_y)$

(e) Beam 1 $\partial Q_x/\partial(2J_y)$

(f) Beam 2 $\partial Q_x/\partial(2J_y)$

Figure 16: Simulation results with b_5, a_5, b_6 and a_6 errors. Measurement results are shown as dashed lines and colored areas, representing the mean and standard deviation respectively.

4 Conclusion

The MD3311 was completed successfully and provided new insights into the sources of amplitude detuning: A large contribution originates from feed-down due to crossing in IP5 and there is much less amplitude detuning present in the flat-orbit configuration. Thanks to the findings, the amplitude detuning seen during commissioning is now better understood. At the same time a 5th order resonance line was probed and the K-modulation procedure could be verified to produce the expected results without any complications.

Simulations have been conducted in the hope to identify specific multipole error components, which can explain the measured detuning behavior. It was found, that due to the large β-functions, the bi-directional orbit distortions and the distribution of errors, all of the investigated multipole orders contribute to detuning and the resulting dependence is complex and entangled. Therefore, with the uncertainties and limitations of the magnetic model, it was not possible to reproduce the measured detuning by simulation perfectly, yet results from simulation and measurement agree well on an order-of-magnitude basis.

The magnetic model is currently being reviewed in collaboration with the magnet group, partly due to the inconsistencies found during this study.

5 Acknowledgements

Many thanks go to the OP and BI groups for the support lent to these studies. An equal amount of gratitude goes out to the collimation team for helping facilitate the large amplitude kicks necessary for nonlinear measurements in the LHC. A whole hearted thank you, to the rest of the OMC team, for being always there for answering questions and providing and updating the Beta-Beating software, without which this analysis would not have been possible. Great thanks to M. Giovannozzi for insightful feedback and very helpful discussion about the content of the note and to G. Arduini for the finishing touches on it.

References

[1] E. H. Maclean, *4.2.2 Amplitude detuning*, in Modelling and Correction of the Non-Linear Transverse Dynamics of the LHC from Beam-Based Measurements, Herford College, University of Oxford, 2014. URL: http://cds.cern.ch/record/1951379.

[2] E. H. Maclean, R. Tomás, F. Schmidt and T. H. B. Persson, *Measurement of nonlinear observables in the Large Hadron Collider using kicked beams*, Phys. Rev. ST Accel. Beams **17** (2014), p. 081002. URL: https://link.aps.org/doi/10.1103/PhysRevSTAB.17.081002, doi:10.1103/PhysRevSTAB.17.081002.

[3] A. Bazzani, G. Servizi, E. Todesco and G. Turchetti, *9.3 Sextupole and octupole first order effect*, in A Normal Form Approach to the Theory of Nonlinear Betatronic Motion, CERN Yellow Reports: Monographs, CERN, Geneva, 1994. URL: http://cds.cern.ch/record/262179.

[4] J. Gareyte, J. P. Koutchouk and F. Ruggiero, *Landau Damping, Dynamic Aperture and Octupoles in LHC*, LHC Project Report 91, CERN, Apr. 1997. URL: https://cds.cern.ch/record/321824.

[5] E. H. Maclean, R. Tomás, M. Giovannozzi and T. H. B. Persson, *First measurement and correction of nonlinear errors in the experimental insertions of the CERN Large Hadron Collider*, Phys.Rev. ST Accel.Beams **18** (2015), p. 121002. URL: https://doi.org/10.1103/PhysRevSTAB.18.121002, doi:10.1103/PhysRevSTAB.18.121002.

[6] M. Albert et al., *Non-linear beam dynamics tests in the LHC*, Accelerators & Technology Sector Note CERN-ATS-Note-2011-052 MD, July 2011. URL: https://cds.cern.ch/record/1366082.

[7] G. Vanbavinckhove et al., *First Measurements of Higher Order Optics Parameters in the LHC*, Accelerators & Technology Sector Note CERN-ATS-2011-160, Sept. 2011. URL: https://cds.cern.ch/record/1382076.

[8] E. H. Maclean et al., *Non-linear beam dynamics tests in the LHC: LHC dynamic aperture MD on Beam 2 (24th of June 2012)*, Accelerators & Technology Sector Note CERN-ATS-Note-2013-022 MD, CERN, Apr. 2013. URL: https://cds.cern.ch/record/1541980.

[9] S. White, E. H. Maclean and R. Tomás, *Direct amplitude detuning measurement with ac dipole*, Phys. Rev. ST Accel. Beams **16** (2013), p. 071002. URL: https://link.aps.org/doi/10.1103/PhysRevSTAB.16.071002, doi:10.1103/PhysRevSTAB.16.071002.

[10] T. Bach et al., *Measurement of amplitude detuning at flat-top and beta*=0.6 m using AC dipoles*, Accelerators & Technology Sector Note CERN-ATS-Note-2013-015 MD, Mar. 2013. URL: https://cds.cern.ch/record/1528610.

[11] R. Tomás, X. Buffat, S. White, J. Barranco and E. H. Maclean, *Collecting amplitude detuning measurements from 2012*, tech. rep., Apr. 2014. URL: https://cds.cern.ch/record/1694666.

[12] E. H. Maclean, F. S. Carlier and J. Coello de Portugal, *Commissioning of Non-linear Optics in the LHC at Injection Energy*, in Proceedings of IPAC, Busan, Korea, 2016, p. 4. URL: https://cds.cern.ch/record/2207446, doi:10.18429/JACoW-IPAC2016-THPMR039.

[13] O. S. Brüning and S. D. Fartoukh, *LHC Report 501: Field Quality Specification for the LHC Main Dipole Magnets*, tech. rep., CERN, Oct. 2001. URL: https://cds.cern.ch/record/522049.

[14] CERN - Accelerator Technology Department, *Windows Interface to Simulation Errors*. URL: http://wise.web.cern.ch/.

[15] E. H. Maclean et al., *Nonlinear optics commissioning in the LHC*, in Evian, 2016, p. 9. URL: https://indico.cern.ch/event/578001/contributions/2366314/attachments/1374391/2158727/2016_EvianPaper.pdf.

[16] E. H. Maclean, F. S. Carlier, K. Fuchsberger, M. Giovannozzi, T. H. B. Persson and R. Tomás, *Report from LHC MD 1391: First tests of the variation of amplitude detuning with crossing angle as an observable for high-order errors in low-beta* colliders*, accelerators & Technology Sector Note, Jan. 2017. URL: http://cds.cern.ch/record/2314409.

[17] E. H. Maclean et al., *New Methods for Measurement of Nonlinear Errors in LHC Experimental IRs and Their Application in the HL-LHC*, in IPAC2017, Copenhagen, Denmark, 2017. URL: https://cds.cern.ch/record/2289663, doi:10.18429/JACoW-IPAC2017-WEPIK093.

[18] E. H. Maclean, F. S. Carlier, M. Giovannozzi, T. Persson and R. Tomás, *Effect of Linear Coupling on Nonlinear Observables at the LHC*, in IPAC2017, Copenhagen, Denmark, 2017. URL: https://cds.cern.ch/record/2289662, doi:10.18429/JACoW-IPAC2017-WEPIK092.

[19] E. H. Maclean et al., *New LHC optics correction approaches in 2017*, Dec. 2017, p. 7. URL: https://indico.cern.ch/event/663598/contributions/2781846.

[20] E. H. Maclean et al., *New approach to LHC optics commissioning for the nonlinear era*, Phys. Rev. Accel. Beams **22** (2019), p. 061004. URL: https://link.aps.org/doi/10.1103/PhysRevAccelBeams.22.061004, doi:10.1103/PhysRevAccelBeams.22.061004.

[21] E. H. Maclean et al., *Detailed review of the LHC optics commissioning for the nonlinear era*, Accelerators & Technology Sector Note CERN-ACC-2019-0029, Feb. 2019. URL: http://cds.cern.ch/record/2655741.

[22] E. H. Maclean, R. Tomas Garcia, T. H. B. Persson and F. S. Carlier, *Report from LHC MD 2171: Amplitude dependent closest tune approach from normal and skew octupoles*, accelerators & Technology Sector Note, 2018. URL: http://cds.cern.ch/record/2310163.

[23] F. S. Carlier et al., *MD2723 - Amplitude Detuning Studies at 6.5 TeV with Various Configurations of the Crossing Scheme*, accelerators & Technology Sector Note, Feb. 2018. URL: http://cds.cern.ch/record/2306325.

[24] E. H. Maclean, *LHC optics commissioning in 2018*, LMC Meeting, May 2018. URL: https://indico.cern.ch/event/733065/contributions/3023327/attachments/1658707/2656509/2018-05-30_LMC_2018commissioning.pdf.

[25] E. H. Maclean, *Nonlinear optics MDs in 2018*, HSS Meeting, Jan. 2018. URL: https://indico.cern.ch/event/779845/contributions/3275039/attachments/1779557/2894503/2019_nonlinearMDs.pdf.

[26] M. Kuhn, V. Kain, G. Trad, R. Tomás, R. Steinhagen and B. Dehning, *New Tools for K-modulation in the LHC*, Accelerators & Technology Sector Note CERN-ACC-2014-0159, June 2014. URL: https://cds.cern.ch/record/1742310.

[27] J. Coello de Portugal, R. Tomás and M. Hofer, *New local optics measurements and correction techniques for the LHC and its luminosity upgrade*, Phys. Rev. Accel. Beams **23** (2020), p. 041001. URL: https://link.aps.org/doi/10.1103/PhysRevAccelBeams.23.041001, doi:10.1103/PhysRevAccelBeams.23.041001.

[28] O. S. Brüning, M. Giovannozzi, S. D. Fartoukh and T. Risselada, *Dynamic aperture studies for the LHC separation dipoles*, Tech. Rep. LHC Project Note 349, CERN, 2004. URL: https://cds.cern.ch/record/742967.

[29] E. H. Maclean et al., *Report from LHC MD 2158: IR-nonlinear studies*, Accelerators & Technology Sector Note CERN-ACC-2018-0021, Mar. 2018. URL: https://cds.cern.ch/record/2306295.

[30] F. S. Carlier, R. Tomás and E. H. Maclean, *Measurement and Correction of Resonance Driving Terms in the LHC*, Be Submitt. (2019).

[31] M. Gasior and R. Jones, *The Principle and First Results of Betatron Tune Measurement by Direct Diode Detection*, 2005. URL: http://cds.cern.ch/record/883298.

[32] CERN - Accelerator Technology Department, *Wise Error Tables for 6.5TeV*, 2015. URL: https://dfsweb.web.cern.ch/dfsweb/Services/DFS/DFSBrowser.aspx/Projects/WISE/Other/Errors/2015-2016/fqrunII2015squeeze0.4_10.0_0.4_3.06.5TeVseeds/.

[33] E. Forest, F. Schmidt and E. McIntosh, *Introduction to the Polymorphic Tracking Code*, SPS and LHC Division Note CERN–SL–2002–044 (AP), July 2002. URL: http://cds.cern.ch/record/573082.

[34] M. G. Minty and F. Zimmermann, *2.8.4 Closest Tune Approach*, in Measurement and Control of Charged Particle Beams, Particle Acceleration and Detection, Springer Berlin Heidelberg, Berlin, Heidelberg, 2003. URL: http://link.springer.com/10.1007/978-3-662-08581-3, doi:10.1007/978-3-662-08581-3.

[35] A. Franchi, S. M. Liuzzo and Z. Marti, *Analytic formulas for the rapid evaluation of the orbit response matrix and chromatic functions from lattice parameters in circular accelerators*, ArXiv Prepr. (2017). arXiv:1711.06589.

[36] E. H. Maclean et al., *Demonstration of coupling correction below the per-mil limit in the LHC*, Accelerators & Technology Sector Note CERN-ACC-NOTE-2016-0053, Aug. 2016. URL: https://cds.cern.ch/record/2210530.

Appendices

A WISE 2015 distribution

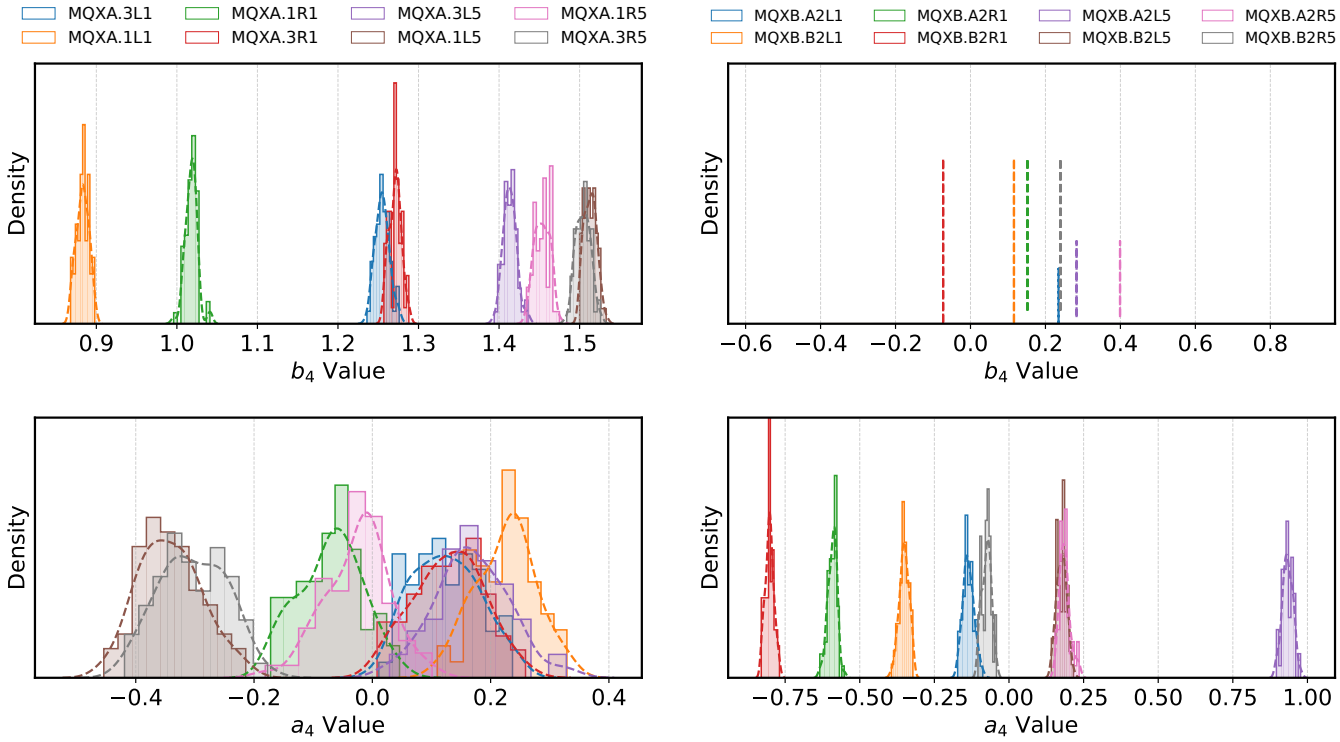

(a) MQXA **(b)** MQXB

Figure 17: Normalized distribution density of b_4 and a_4 errors of the 60 seeds of the 2015 WISE error tables for 6.5 TeV [32]. Values are shown for the quadrupole magnets of the IP1 and IP5 triplets, separated into MQXA (left column) and MXQB (right column). The dashed lines show the kernel density estimation of the respective distribution. For b_4 in the MQXB there is only the constant systematic error value throughout the seeds, indicated by the straight lines.

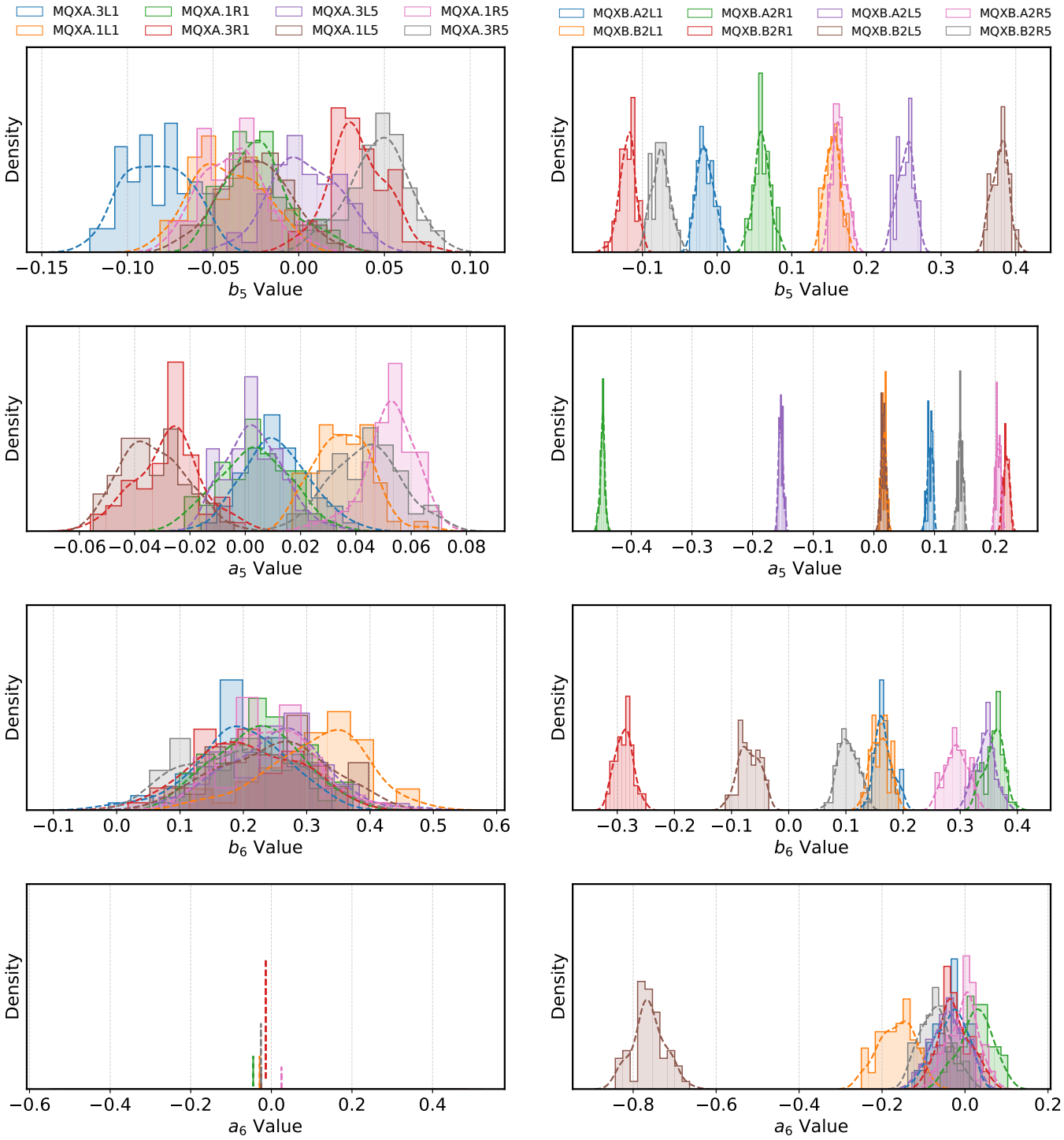

(a) MQXA **(b)** MQXB

Figure 18: Normalized distribution density of b_5, a_5, b_6 and a_6 errors of the 60 seeds of the 2015 WISE error tables for 6.5 TeV [32]. Values are shown for the quadrupole magnets of the IP1 and IP5 triplets, separated into MQXA (left column) and MXQB (right column). The dashed lines show the kernel density estimation of the respective distribution. For a_6 in the MQXA there is only the constant systematic error value throughout the seeds, indicated by the straight lines.

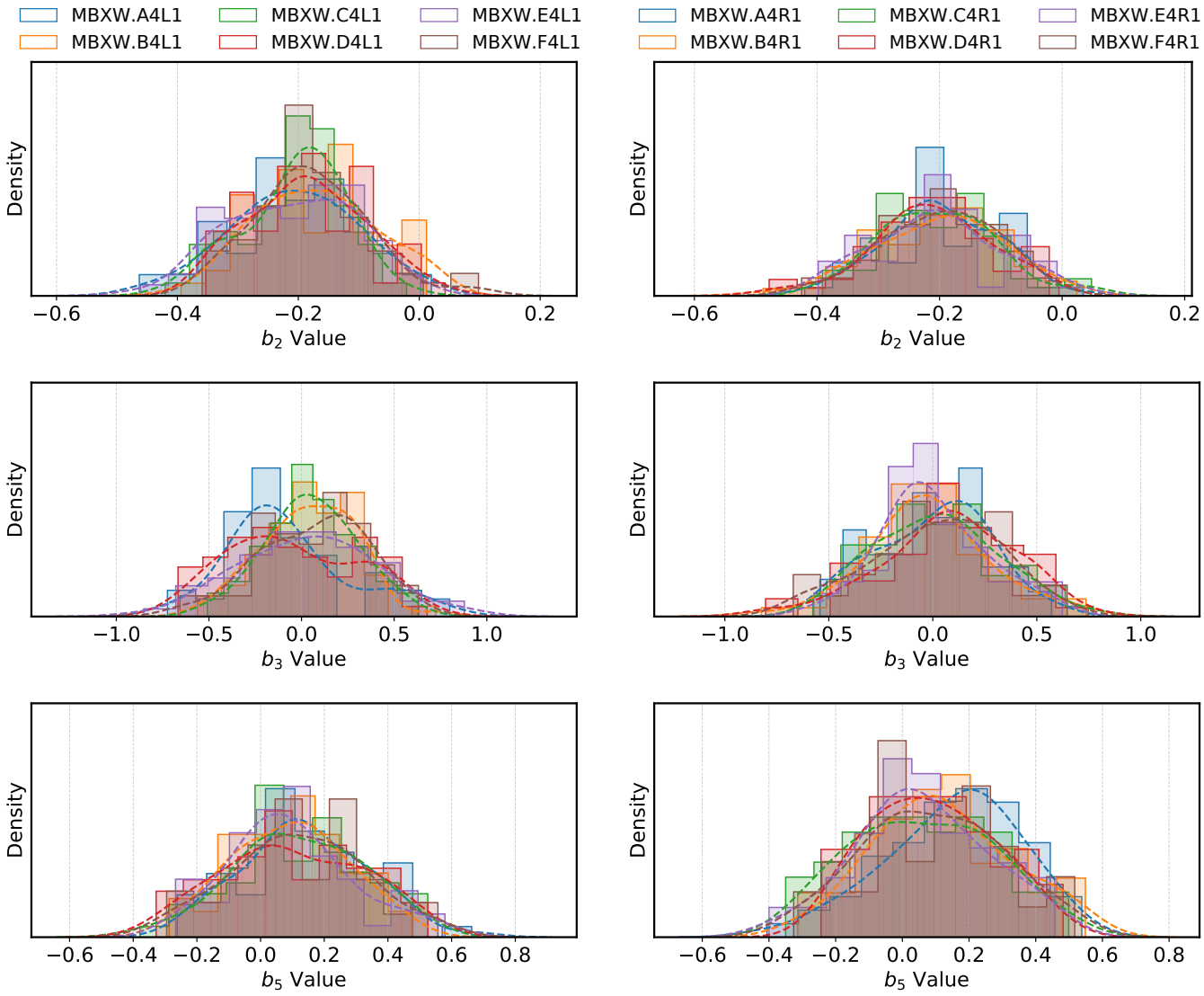

(a) MBXW left of IP1

(b) MBXW right of IP1

Figure 19: Normalized distribution density of b_2, b_3 and b_5 errors of the 60 seeds of the 2015 WISE error tables for 6.5 TeV and squeezed 40 cm optics [32]. Values are shown for the MBXW (D1) magnets of IP1, separated into left of IP1 (left column) and right of IP1 (right column). The dashed lines show the kernel density estimation of the respective distribution. All other orders of field error are zero in the WISE tables.

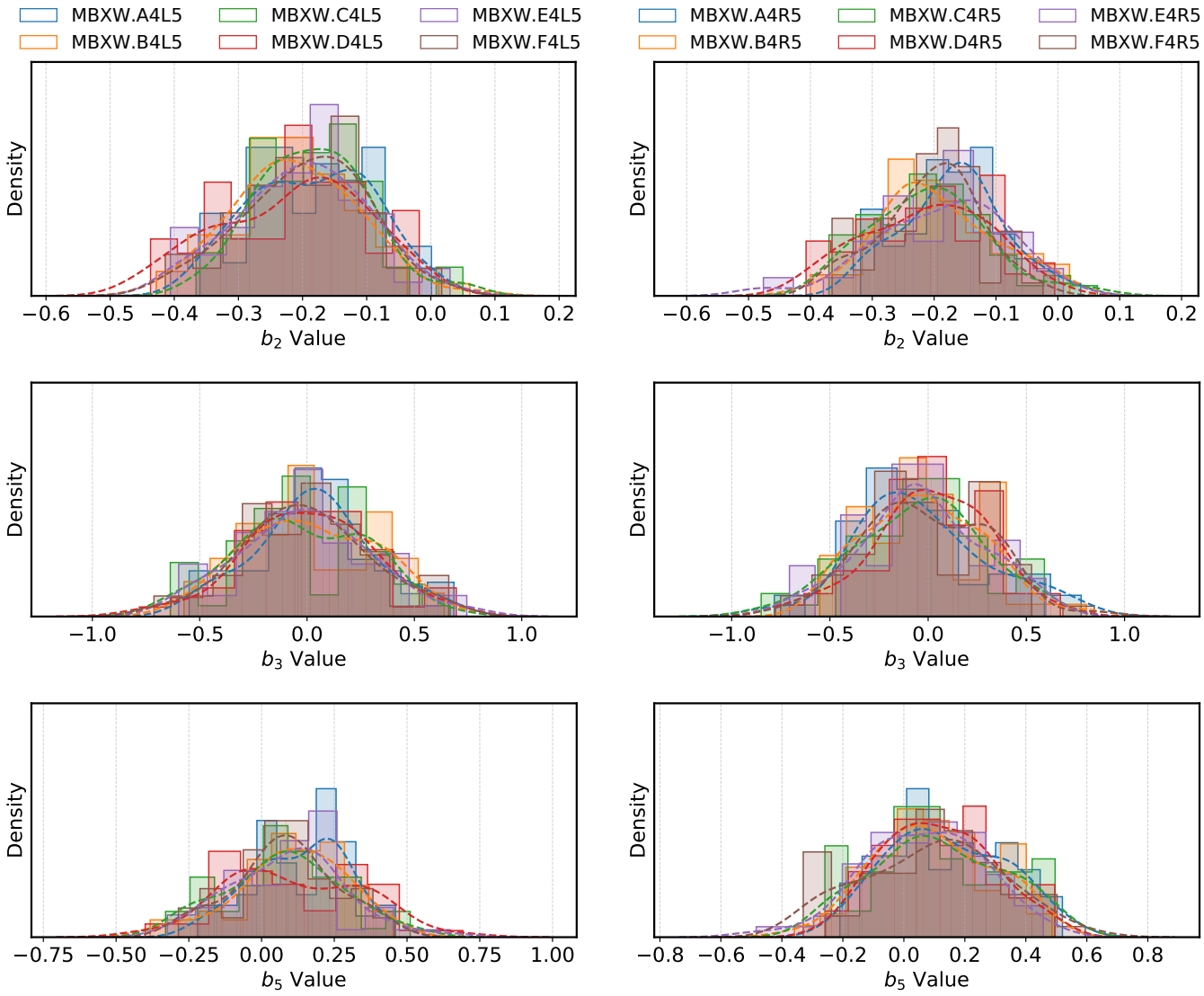

(a) MBXW left of IP5

(b) MBXW right of IP5

Figure 20: Normalized distribution density of b_2, b_3 and b_5 errors of the 60 seeds of the 2015 WISE error tables for 6.5 TeV and squeezed 40 cm optics [32]. Values are shown for the MBXW (D1) magnets of IP5, separated into left of IP5 (left column) and right of IP5 (right column). The dashed lines show the kernel density estimation of the respective distribution. All other orders of field error are zero in the WISE tables.

B Second Order Amplitude Detuning

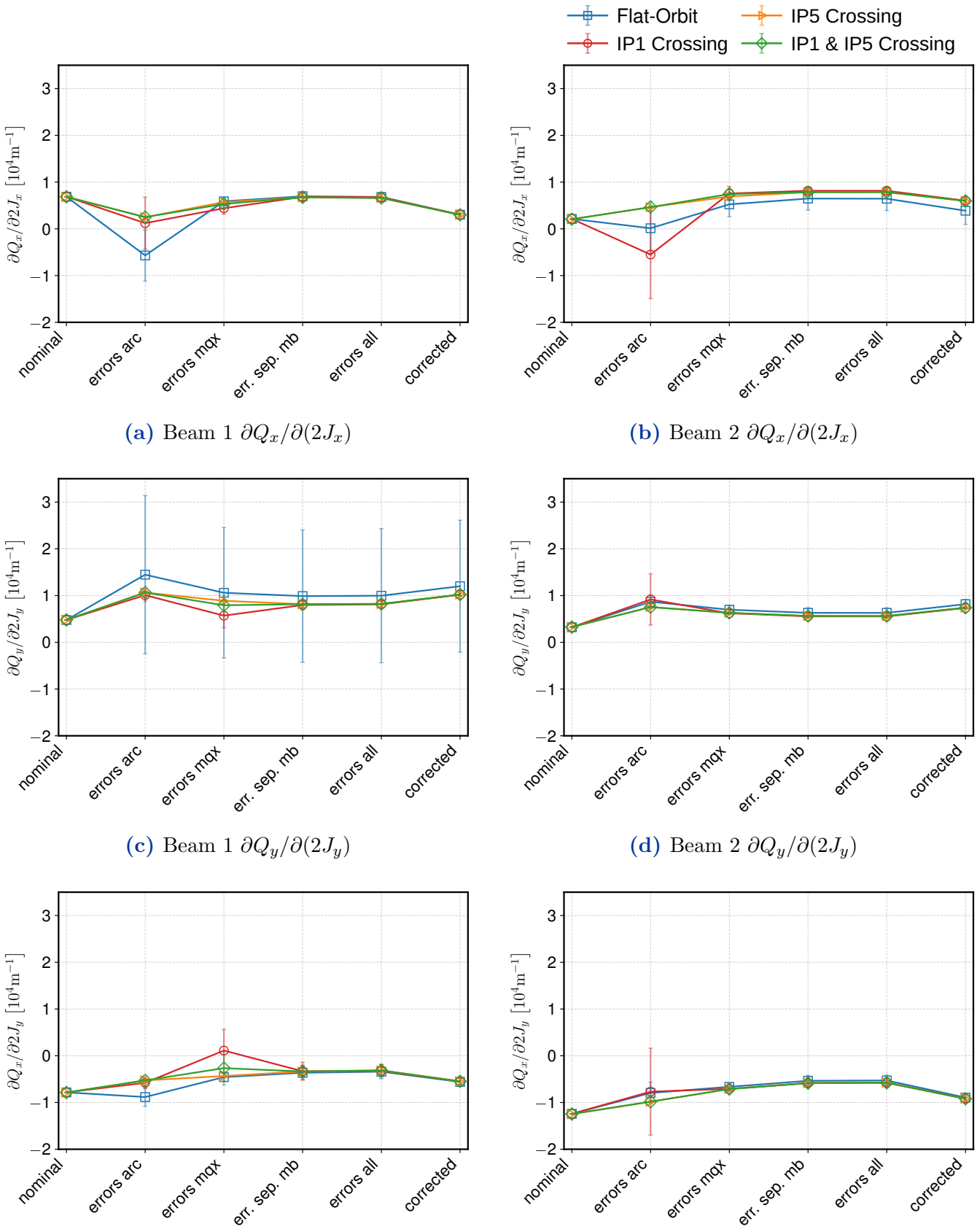

(a) Beam 1 $\partial Q_x/\partial(2J_x)$

(b) Beam 2 $\partial Q_x/\partial(2J_x)$

(c) Beam 1 $\partial Q_y/\partial(2J_y)$

(d) Beam 2 $\partial Q_y/\partial(2J_y)$

(e) Beam 1 $\partial Q_x/\partial(2J_y)$

(f) Beam 2 $\partial Q_x/\partial(2J_y)$

Figure 21: Simulation results with only b_3 errors. Coupling has been corrected throughout these simulations.